Article

Cell

Temporal Stability of the Human Skin Microbiome

Graphical Abstract

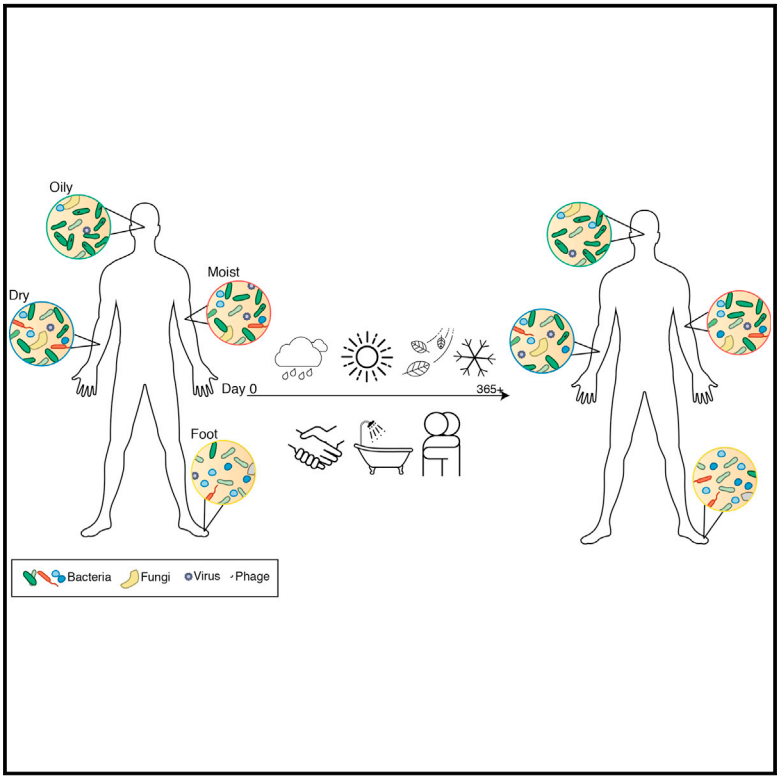

Authors

Julia Oh, Allyson L. Byrd, Morgan Park, NISC Comparative Sequencing Program, Heidi H. Kong, Julia A. Segre

Correspondence

konghe@mail.nih.gov (H.H.K.), jsegre@mail.nih.gov (J.A.S.)

In Brief

Healthy adults stably maintain their skin microbial communities over time at the kingdom, phylum, species, and even, strain level, despite constant exposure to the external environment and other individuals.

Highlights

- Composition of skin microbiome (bacteria, fungi, and viruses) is shaped by physiology
- Conservation of skin microbial communities can vary by site and individual
- Skin microbial communities are stable at the strain level, despite external exposures
- Eukaryotic viruses are the most transient members of the skin community

Oh et al., 2016, Cell *165*, 854–866
May 5, 2016
http://dx.doi.org/10.1016/j.cell.2016.04.008

CellPress

Cell

Article

Temporal Stability of the Human Skin Microbiome

Julia Oh,[1,5,7] Allyson L. Byrd,[1,2,5] Morgan Park,[3] NISC Comparative Sequencing Program,[3] Heidi H. Kong,[4,6,*] and Julia A. Segre[1,6,*]

[1]Translational and Functional Genomics Branch, National Human Genome Research Institute, NIH, Bethesda, MD 20892, USA
[2]Department of Bioinformatics, Boston University, Boston, MA 02215, USA
[3]NIH Intramural Sequencing Center, National Human Genome Research Institute, Bethesda, MD 20892, USA
[4]Dermatology Branch, Center for Cancer Research, National Cancer Institute, NIH, Bethesda, MD 20892, USA
[5]Co-first author
[6]Co-senior author
[7]Present address: The Jackson Laboratory for Genomic Medicine, Farmington, CT 06030, USA
*Correspondence: konghe@mail.nih.gov (H.H.K.), jsegre@mail.nih.gov (J.A.S.)
http://dx.doi.org/10.1016/j.cell.2016.04.008

SUMMARY

Biogeography and individuality shape the structural and functional composition of the human skin microbiome. To explore these factors' contribution to skin microbial community stability, we generated metagenomic sequence data from longitudinal samples collected over months and years. Analyzing these samples using a multi-kingdom, reference-based approach, we found that despite the skin's exposure to the external environment, its bacterial, fungal, and viral communities were largely stable over time. Site, individuality, and phylogeny were all determinants of stability. Foot sites exhibited the most variability; individuals differed in stability; and transience was a particular characteristic of eukaryotic viruses, which showed little site-specificity in colonization. Strain and single-nucleotide variant-level analysis showed that individuals maintain, rather than reacquire, prevalent microbes from the environment. Longitudinal stability of skin microbial communities generates hypotheses about colonization resistance and empowers clinical studies exploring alterations observed in disease states.

INTRODUCTION

Human skin is the first line of defense against pathogens, while simultaneously harboring a diverse milieu of commensals, including bacteria, fungi, and viruses. These symbiotic organisms play essential roles in lipid metabolism, colonization resistance to transient organisms, and education of the immune system (Belkaid and Segre, 2014; Grice, 2015; Scharschmidt and Fischbach, 2013). Previous studies have shown strong site specificity microbial community composition and function: the physiologic characteristics of a skin site, including pH, temperature, moisture, sebum content, and topography, shape the local microbial community (Costello et al., 2009; Findley et al., 2013; Grice et al., 2009; Grice and Segre, 2011; Oh et al., 2014). Understanding community variability across skin sites has provided the foundation to study the corresponding site specificity of disease predilection, for example, atopic dermatitis (eczema) in the bends of the arms and legs (Kong et al., 2012) and psoriasis on the elbows and knees (Alekseyenko et al., 2013). However, it is poorly understood why disease predilection changes over human lifespans and whether fluctuations in host-intrinsic factors, such as immunity or hygiene, influence microbial community composition and function. Understanding stability determinants is critical to studies investigating if homeostatic forces contribute to a healthy skin microbial community and if alterations influence host health.

In addition to skin's biogeography, as defined by physiologic factors, such as sebaceous, moist, or dry, individual discriminatory attributes also likely contribute to skin microbial community dynamics over time. Using the high-resolution and multi-kingdom analyses afforded by metagenomic shotgun sequencing, we have shown that low-abundance microbial species, including bacteria, fungi, and viruses, can differentiate between individuals. Observing interkingdom dynamics is meaningful since these interactions may exacerbate disease severity (Peleg et al., 2010) or facilitate transitions from opportunistic to pathogenic. Moreover, a subspecies-level analysis of dominant skin species showed that strains can be unique to an individual, while the population heterogeneity of other species can be more specific to skin physiology (Oh et al., 2014). Distinguishing between strains of the same species is necessary because some strains are beneficial, while others may be pathogenic to the host.

Shotgun sequencing data provide resolution difficult to achieve with phylogenetic marker gene analyses. Metagenomic surveys of the gut have shown that single-nucleotide variants (SNVs) (Schloissnig et al., 2013) and gene copy-number variations (Greenblum et al., 2015; Zhu et al., 2015) can identify individual-specific strains, which illustrate functional differences that cannot be explained by species composition alone. Longitudinal studies in the gut have found individual-specific strains persist for a year (Schloissnig et al., 2013) or more (Faith et al., 2013). These studies have leveraged a combination of compositional and functional attributes to identify a broad trend of long-term retention of one's individual strains over time, even at the SNV level.

To understand community dynamics of healthy human skin, we investigated the temporal stability and diversity of skin microbial communities, expanding our previous metagenomic study

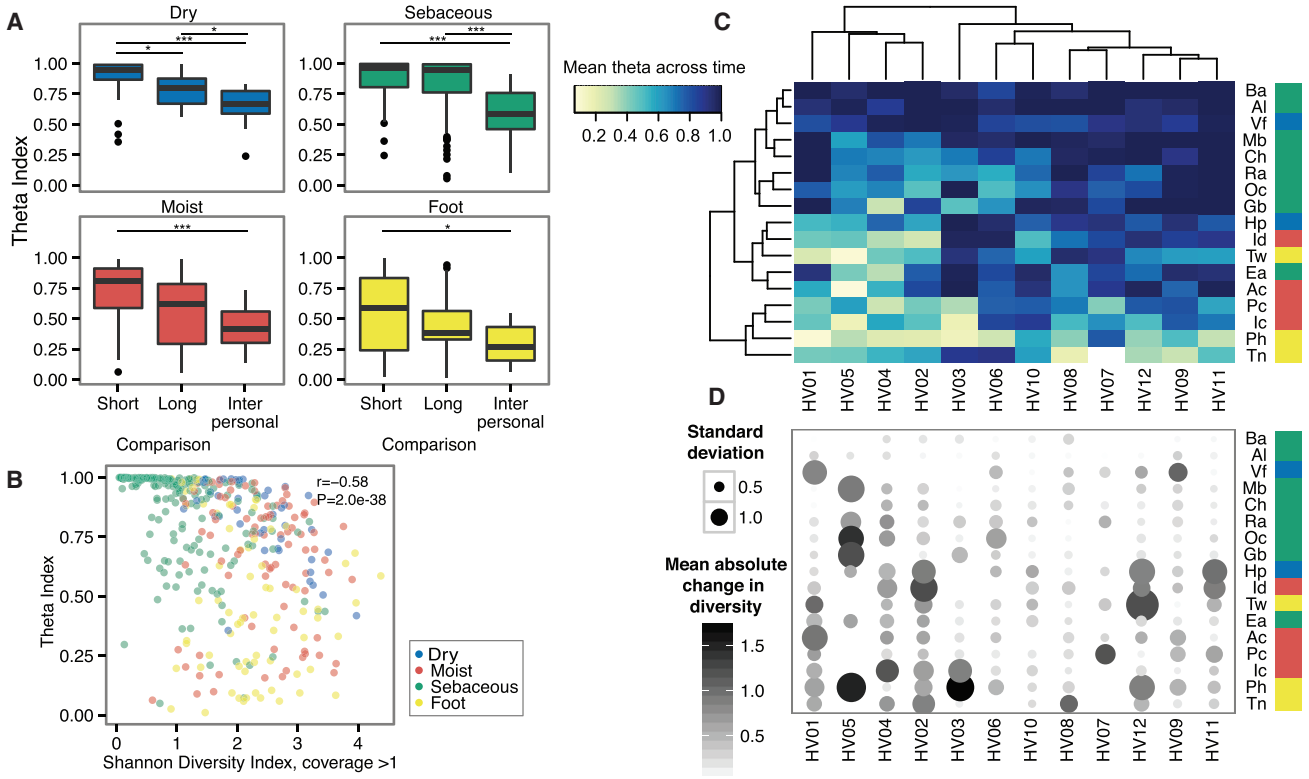

Figure 1. Community Stability Is Dependent on Both Site and Individuality

(A–D) Sites are color-coded by characteristic and defined in Figure S1. (A) Boxplots of Yue-Clayton theta indices calculate similarity between sites aggregrated by characteristic. "Long" duration indicates ~1–2 years between samplings; "short" duration averages 1 month (T2 to T3). For comparison, "interpersonal" values show the average between individuals. Bonferroni-adjusted *p < 0.05 value, **p < 0.01 value, ***p < 0.001 value. (B) Quantification of community stability relative to community diversity by partial Spearman correlation. Diversity is measured by the Shannon diversity index, calculated for genomes with coverage greater than one. (C) Hierarchical clustering (complete linkage) of mean theta indices over the average of "long" and "short" values for each individual at each site sampled. (D) Mean change in community diversity over time, ordered as in (C) to show that community stability tracks with stability in diversity. Circle size shows the SD of diversity, and color indicates magnitude of changes in diversity. HV, healthy volunteer.

See also Figure S1.

to resample individuals at successive time points. Here, we show that community stability persists regardless of the sampling time interval and despite constant exposure of skin communities to extrinsic factors. Interestingly, the nature and degree of this stability is highly individual specific, a trend previously observed with phylogenetic marker gene sequencing across body sites (Flores et al., 2014; Gajer et al., 2012). Strain-level analysis reveals that this stability is driven primarily by the maintenance of individual strains over time, rather than through the acquisition of prevalent microbes from the environment and other individuals (Lax et al., 2014). We present new insights into how biogeography and individuality affects stability and transience of the skin microbiome community.

RESULTS

Skin Microbes Are Largely Stable at a Community Level

Our previous studies defined that the diversity and composition of skin microbial communities possess both site- and individual-specific qualities (Oh et al., 2014). To assess the effect of time on these characteristics, we collected samples over long (1–2 years) and short (1–2 months) time intervals. 12 healthy individuals were sampled across 17 skin sites at three time points for a total of 594 samples and 720 Gbp of shotgun microbial sequence data (Figures S1A and S1B). For taxonomic reconstructions, we mapped microbial reads to a multi-kingdom reference database. To assess the stability of skin microbial communities, we compared community membership and structure over short and long time intervals using the Yue-Clayton theta index, which calculates the distance between communities based on relative proportions of shared and non-shared species in each population (Yue and Clayton 2005). $\theta = 0$ indicates dissimilar and $\theta = 1$ identical communities. We observed that an individual's short- and long-term community similarity significantly exceeded similarity between individuals (Figures 1A and S1A), similar to observations in gut and other communities (Caporaso et al., 2011; Costello et al., 2009; Faith et al., 2013; Flores et al., 2014; Human Microbiome Project Consortium, 2012). At all sites, long-term was lower than short-term similarity at the species level, a trend also observed when comparing timescales of 1 day versus 3 months (Costello et al., 2009). Bacterial and fungal communities of sebaceous sites were the most stable regardless

of time intervals. Surprisingly, dry sites, including high-exposure, high-perturbation sites, such as the palm, were also stable regardless of time. Foot sites were the least stable, with significant differences over both the short- and long-term. This may be due to a combination of behavioral and physiologic factors, including shoe-wearing habits, personal hygiene, or features such as the thickness of plantar stratum corneum (the upper layer of skin). We also examined stability at higher taxonomic levels to ask what level of taxonomic resolution contributes most to stability. We observed similar trends of long- and short-term stability to the phylum level, and differences in short and long-term stability disappeared at the kingdom level (data not shown).

We investigated next whether stability over time is linked to different community traits, such as diversity. Stability was modestly anti-correlated with community diversity (Figure 1B) as measured by the Shannon diversity index, which measures both species richness and evenness. This suggested that high-diversity sites (foot, moist) were likely to be less stable than low-diversity (primarily sebaceous) sites, consistent with previous reports (Grice et al., 2009). We then asked if skin communities typically reach and maintain species saturation over time, which could reflect constancy in community diversity over time. Here, we examined trends of longitudinal diversity on a per-site, per-individual basis. No site exhibited statistically significant trends of diversity changes over time ($p > 0.05$, all sites). This suggested that community diversity is generally homeostatic in these healthy individuals, and if changes in the community occur over time, species may be replaced by similar types and numbers, preserving overall niche characteristics.

In certain individuals, we observed large shifts in diversity at multiple sites. This suggested that while skin microbial communities overall exhibit site-specific trends in stability, stability itself may be largely an individual trait that has been observed previously in skin, gut, and vaginal communities (Flores et al., 2014; Gajer et al., 2012). To assess this, we clustered communities to identify potential individual-specific patterns in stability. Two-way hierarchical clustering of mean theta indices over time showed that sebaceous sites were stable regardless of the individual, while foot and moist sites tended to be more variable, as previously observed (Figure 1C). However, we defined a cluster comprised of 4/12 individuals (HV01, HV02, HV04, and HV05) as "high variability," because even at stereotypically stable sites (e.g., sebaceous), their communities tended to fluctuate more. This variability was even more pronounced at moist and dry sites. We then examined whether length of time between sampling was associated with this increased variability, as longer time intervals might increase stochastic drift and perturbation. Surprisingly, we observed no significant change in community composition or in magnitude of diversity as a function of days between "long" sampling time intervals (Figures S1C and S1D). While certain sites (e.g., moist) trended toward increased variability as a function of time, we believe that individual factors may play a role in defining stability. We observed a similar trend when incorporating changes in community diversity over time (Figure 1D). "High-variability" individuals also tended to have greater shifts in community diversity over time. Such shifts could reflect greater responsiveness to intrinsic or extrinsic perturbation events, for example, conditions that favor expansion of a limited set of species, bottleneck events, or large-scale selective sweeps at certain sites in these individuals.

Diverse Signatures of Skin Microbe Stability at the Species Level

We then sought to identify if specific species or community types are intrinsically unstable in the skin niche or if increased variability is a phenomenon in which many species flux simultaneously in a community. For example, if a species is poorly adapted to a skin niche, relative abundances could vary significantly over time with growth competition. Or, in antagonistic interspecies relationships, cyclic changes in relative abundance could also occur. Community composition, describing the relative abundances of bacteria, fungi, and DNA viruses across samples, confirmed that skin communities are largely stable over time (Figures 2A and S2A). Of communities that tended to be less stable, we asked whether certain species were more likely to contribute to instability. Correlation analysis of relative abundances of skin species between time points in these sites showed that "high-flux" species, those that fluctuated more over time, differed by site and individual (Figure 2B). For example, in the dry hypothenar palm (Hp), we observed that *Propionibacterium acnes* was a high-flux organism for multiple individuals. In the moist popliteal crease, *Polyomavirus HPyV7* was a high-flux species for one individual, *Polyomavirus HPyV6* for another, and *Staphylococcus epidermidis* for yet another. In the high-instability plantar heel, abundances of *S. hominis*, *S. epidermidis*, and *Alphapapillomavirus* changed significantly over time. While these species may flux in certain individuals and sites, most skin microbes appeared intrinsically stable. Thus, a complex interaction of host status and environmental perturbations likely influences these local changes in skin communities.

We also examined phage-host relationships as a potential interspecies source of variability in microbial communities. While mixed phage-bacterial communities were typically stable (Figures 2A and S2A), we observed instances of large-scale shifts in phage-bacteria ratios that could reflect a perturbation event, e.g., HV12. We investigated the relative abundances of the most common phages in skin (Figures 2C and S2B) to search for relationships that might provide clues about bacteria-phage interactions. Both *P. acnes* and *Propionibacterium* phage are abundant in sebaceous sites, and we observed a strong anti-correlation in sebaceous communities that contain both *P. acnes* and its phage (Figure 2C). While the compositional (versus absolute) nature of the data means that taxon abundances are not perfectly independent, this anti-correlation together with the observed phage-host dynamics over time suggests antagonism.

We also observed multiple populations of *P. acnes* that had a neutral or positive correlation with *Propioinibacterium* phage abundance (Figure S2B, points along x axis), potentially reflecting variability of *P. acnes* strains in skin communities in which some strains may be interacting with phages and others may not (Liu et al., 2015). Similar findings were also evident in dry and moist sites, most notably in the feet in which a positive correlation was observed. On the feet, *Propionibacterium* phages

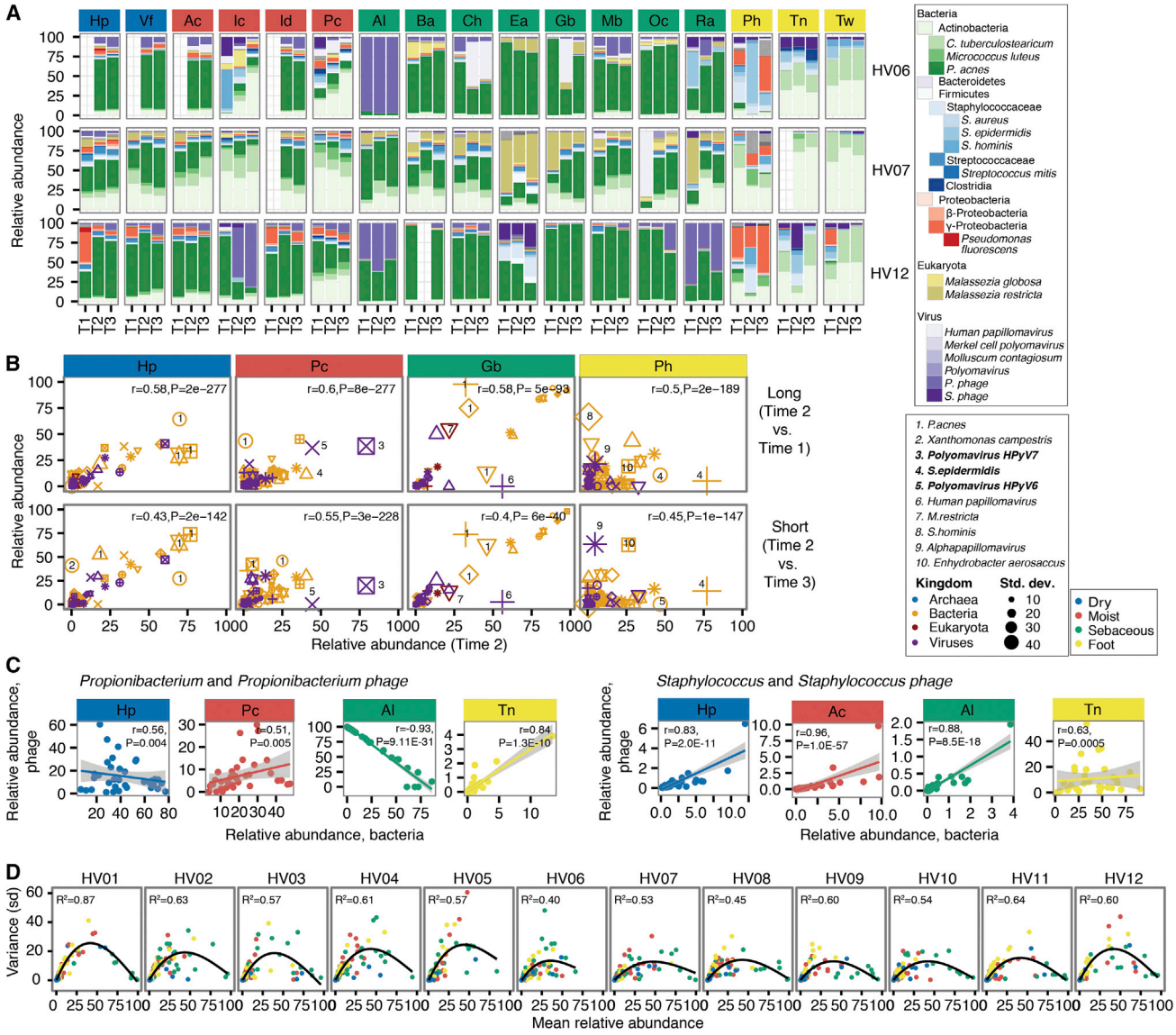

Figure 2. Community Stability Is Defined by Different Species Characteristics, Depending on Site and Individual

(A–D) For all panels, sites are color-coded by site characteristic. (A) Relative abundances of the most common skin bacteria, fungi, and viruses are shown for three representative individuals. A full set of taxonomic classifications is shown in Figure S3. T1, T2, and T3 indicate order in the time series. (B) Correlating taxon abundances for the "long" versus "short" time series for select sites from (A) that showed higher variability. Different shapes represent different individuals; different colors represent kingdom of species, and size of point indicates species SD between samples. Select abundant taxa (five most highly variable) are numbered as indicated. Partial Spearman correlations adjusting for repeated measures with associated p values are in the upper right. (C) Phage and host dynamics at select sites. For *Propionibacterium acnes* and *Staphylococcus*, relative abundances of phage versus bacteria are plotted for each sample. A linear model was fitted to the data with shading showing the 95% confidence interval for the goodness of fit. To quantify correlation or anticorrelation, partial Spearman correlation coefficients and associated adjusted p values were calculated. (D) The relationship between taxon abundance and variance, measured as SD, is shown for taxa >0.25% relative abundance in the population. A generalized additive model, showing a second-order relationship, was fitted to the data to generate correlation coefficients (upper left). All p values < 0.05. HV, healthy volunteer.

See also Figure S2.

may interact with different *Propionibacterium* species (e.g., *humerusii*), or they may exist in a lysogenic versus a primarily lytic state in sebaceous sites. Relative abundances of *Staphylococcus* and *Streptococcus* phages were largely positively correlated with *Staphylococcus* and *Streptococcus*, suggesting that these may be prophages.

Finally, we examined species abundance as a predictor of stability over time (Figure 2D). We observed a second-order, power-law relationship between taxon mean relative abundance across time and variance, excluding transient species (taxa that disappear from one time point to the next) (Ma 2015). Both low- and high-abundance species had low variance, and the largest

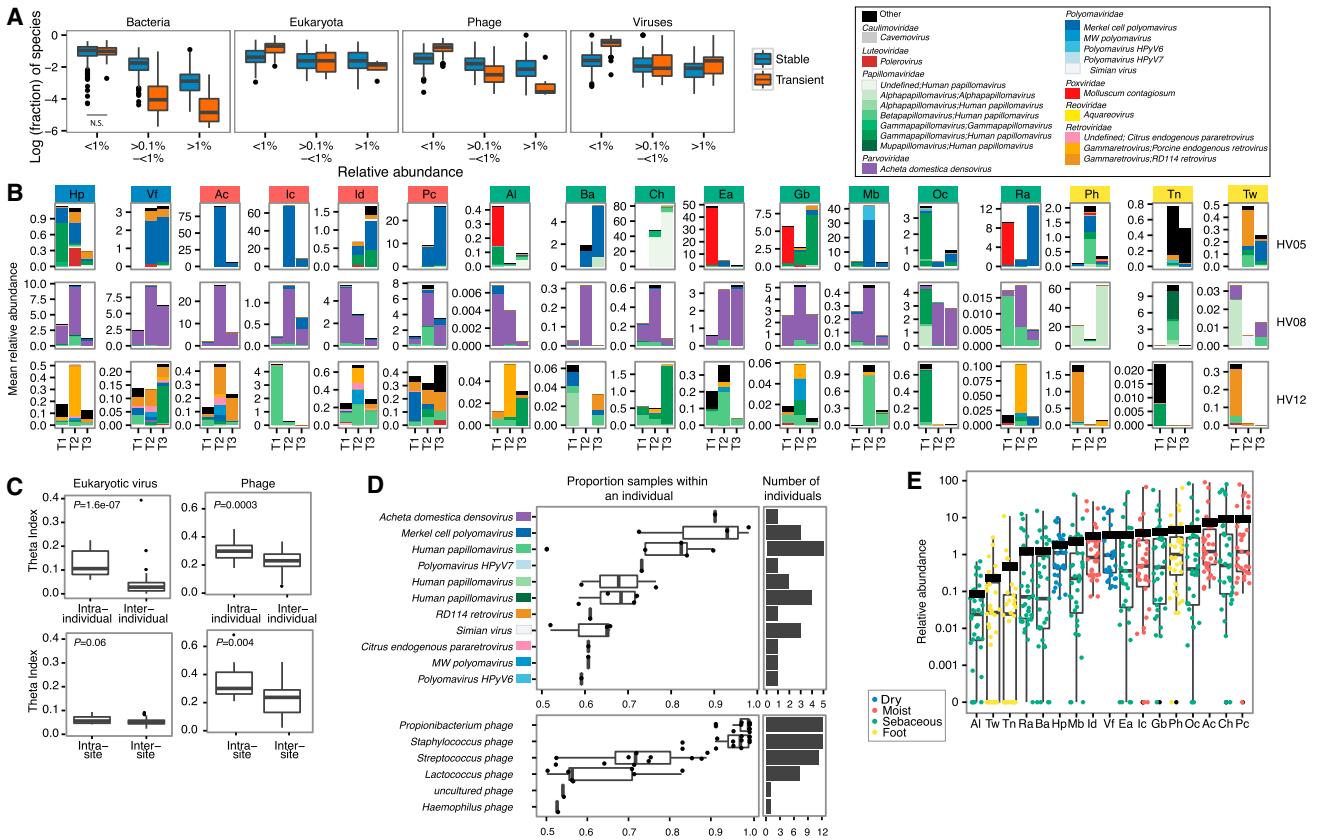

Figure 3. Assessment of Transient versus Non-transient Species across Time by Kingdom and Eukaryotic Viral Stability in the Skin

(A and B) Sites are color-coded by site characteristic. (A) Fraction of species transient or non-transient for each complete longitudinal set of sites per individual. Transience, defined as present in only one of three time points, is measured at three ranges of abundances. All comparisons are adjusted p value <0.05 between transient/non-transient, except for <0.1% Bacteria, which is not significant (ns). (B) Relative abundances of the most common predicted eukaryotic viruses are shown for three representative individuals. A full set of classifications is shown in Figure S3. T1, T2, and T3 indicate order in the time series.

(C) Predicted eukaryotic viruses tend to be individual specific, with significantly more sharedness, calculated with the Yue-Clayton theta coefficient, within an individual than between individuals and with little site specificity. p value, Wilcoxon rank-sum test shown in left corner.

(D) Coreness of predicted eukaryotic viruses. Boxplots and overlaid points show the proportion of samples within an individual in which a virus is observed, with a cutoff of >50% occurrence. The color-coding for lineage is based on the legend in (B). Right: number of individuals in which a eukaryotic virus is observed.

(E) Relative abundance of eukaryotic viruses arranged by site with each individual's value overlaid and colored by site characteristic. The thick black line indicates mean relative abundance of total (eukaryotic and bacterial) DNA viruses at that site.

variance was observed in intermediate abundance species. This second-order relationship was present whether site or individual was used to track species, supporting that this intrinsic property of abundance is not determined solely by species identity. This suggests a broader ecological context in which high-abundance species can be considered "fixed" in the community, and a limited assortment of rare (but not transient) species can also stably persist. Overall, dominant community characteristics, such as diversity and composition, are largely stable over time, where primary determinants of stability are site and individual specificity, with different species contributing to variation in the community over time.

Transience and Eukaryotic dsDNA Viral Stability

Because transient species also likely contribute to community variations over time, we next examined the fraction of the skin community that was transient, i.e., species that were below the detectable range between time points. Because technical limitations, including sampling depth, sequencing depth, and amplification bias, can influence detection particularly at low relative abundances, we measured transience at three abundance ranges (<0.1%, ≥0.1% to ≤1%, >1%) and required a species to occur in that range in at least one time point (Figure 3A). Of very low-abundance organisms (<0.1% relative abundance), a significantly higher fraction consisted of transient organisms from all kingdom classes, except for bacteria, yet this could be partially attributed to reduced robustness in species classification of fungi and viruses at this abundance threshold. For higher abundance ranges, the proportion of stable species significantly exceeded the number of transient organisms for bacteria, fungi, and phages, suggesting that at higher abundances, species from these kingdoms were more likely to be stable residents.

Noteworthy, we observed that double-stranded eukaryotic DNA viruses had a significantly greater fraction of species that

were transient at the higher abundance classes (0.1%–1% and >1%), in striking contrast to the stable residences of bacteria, fungi, and phages (Figure 3A). This is consistent with previous studies in which viral communities were more unstable than the whole metagenome (Hannigan et al., 2015). Types of eukaryotic viruses identified in skin were relatively few (less than two dozen; Figure S3A), with large fluctuations in the number of species observed in some individuals. The taxonomic characterization of these viruses showed three major classes of communities (Figures 3B and S3B). We observed a "uniform" phenotype, in which the viral communities at all sites were predominantly a single viral type (Figure 3B; e.g., HV08). In an "intermediate" phenotype, we observed a dominant species in a large number of sites but high diversity at other sites (Figure 3B; e.g., HV05). In a "variable" phenotype, viral communities tended to differ markedly from site to site and over time (Figure 3B; e.g., HV12) at low abundances. The lack of site specificity in viruses was reflected in comparisons using the theta index (Figure 3C; e.g., HV12), where eukaryotic viral communities were highly dissimilar between sites. Moreover, individuals tended to harbor a unique virome (Figure 3C), with intrapersonal similarity significantly exceeding interpersonal similarity.

Unlike bacterial and fungal species like *P. acnes* and *Malassezia globosa*, which are nearly universal both between and within individuals, we observed little evidence of a core virome in our cohort, although human polyomaviruses and papillomaviruses were identified in approximately half of our subjects (Figure 3D, top). Generally, the most abundant viruses in our cohort were specific to single individuals, including retroviruses, which may be stably incorporated into the host human genome. By contrast, we observed the presence of a strong core phageome (Figure 3D, bottom), in which *Propionibacterium*, *Staphylococcus*, and *Streptococcus* phages were nearly universal between and within individuals. This underscores differences in host specificity in which phages are likely obligate partners with a community's abundant bacterial species and thus have site specificity, while eukaryotic viruses do not (Figure 3C). As viral databases improve and expand, we anticipate that strain resolution of phages and eukaryotic viruses will further refine these interkingdom interactions.

Because eukaryotic viruses inhabiting the human body presumably infect human cells, we inquired if different skin sites had different abundances of eukaryotic viruses. For example, the thick skin of the foot might harbor fewer detectable viruses than a moist site, whose thinner layers may be more susceptible to skin barrier breaks. While shotgun sequencing methodologies prevent estimation of true abundances, we can gain some insight from the proportion of the community comprised of viral sequences. A significant increase in detectable viral DNA could signify a viral bloom relative to the bacterial and fungal community. Note that we observed no consistent trend with amount of human DNA recovered (data not shown), which could have skewed viruses recovered with higher or lower numbers of active human cells obtained in collection.

We created a ranked distribution of eukaryotic viral relative abundances stratified by skin site (Figure 3E). Certain sites, including alar crease, toeweb, toenail, retroauricular crease, and back, had a large fraction of samples with no viral representation and lower relative abundance than did other sites. Sites with modestly higher viral relative abundances were moist skin creases, such as the popliteal and antecubital fossae (as well as adjacent sites on the forearm and palm), cheek, and occiput. But we observed little uniformity in what viruses tended to be higher in relative abundance at these sites; in most individuals, higher viral relative abundances could be attributed to a diversity of polyomaviruses or papillomaviruses. Interestingly, the composition and presence of eukaryotic viruses in skin communities appeared less dependent on physiologic characteristics that strongly shape bacterial and fungal communities; these dynamics may depend more on host status and topography than on nutrient availability.

Individual-Specific Signatures Are Shared across Time and Space

As overall stability is likely an individual trait, with the degree of stability and involved species varying between individuals, we next investigated whether individuals retain unique taxonomic signatures that would allow them to be distinguished from other individuals at different points in time. Recent research has suggested that individuals might possess distinguishing microbial fingerprints that are stable over time (Franzosa et al., 2015). Here, we used a supervised random forest algorithm (Liaw and Wiener, 2002) for each time point to identify key taxa that could differentiate individuals and to identify if these taxa remained the same at each time point. Comparing classifier strength (mean decrease in accuracy) over the different time points, we observed that, surprisingly, a relatively small number of species retained their discriminatory power over time (Figure 4). Low-abundance (<5% relative abundance) organisms were typically those with the highest resolving power between individuals, for example, *Merkel cell polyomavirus*, *Gardnerella vaginalis*, and *Acheta domestica densovirus* (top half of Figure 4, right panel). These organisms also tended to be stable in relative abundance over time with low coefficients of variation (Figure 4, right) and were present at the most sites within an individual across time (Figure 4, center). Species with minimal discriminatory power between individuals (bottom half of Figure 4) were characterized as lacking ability to discriminate individuals at one or more time points, having low prevalence across body sites, and having high variance in their relative abundances over time. The limited ability of species to discriminate individuals over time has been previously described by (Franzosa et al. (2015), who found strain-level codes were more robust to temporal variability.

Individuals Have Distinct Microbial SNV Signatures that Are Stable over Time

Shotgun metagenomic data empower unprecedented resolution of microbial communities at the strain and SNV level. To explore stability at this high resolution, we focused on the prevalent skin bacterial commensals *Propionibacterium acnes* and *Staphylococcus epidermidis*, which have dozens of available genome sequences (Conlan et al., 2012; Tomida et al., 2013). Previously, by mapping shotgun metagenomic reads to this reference set of phylogenetically diverse genomes, we identified that skin sites harbor complex subspecies variation for both *P. acnes* and

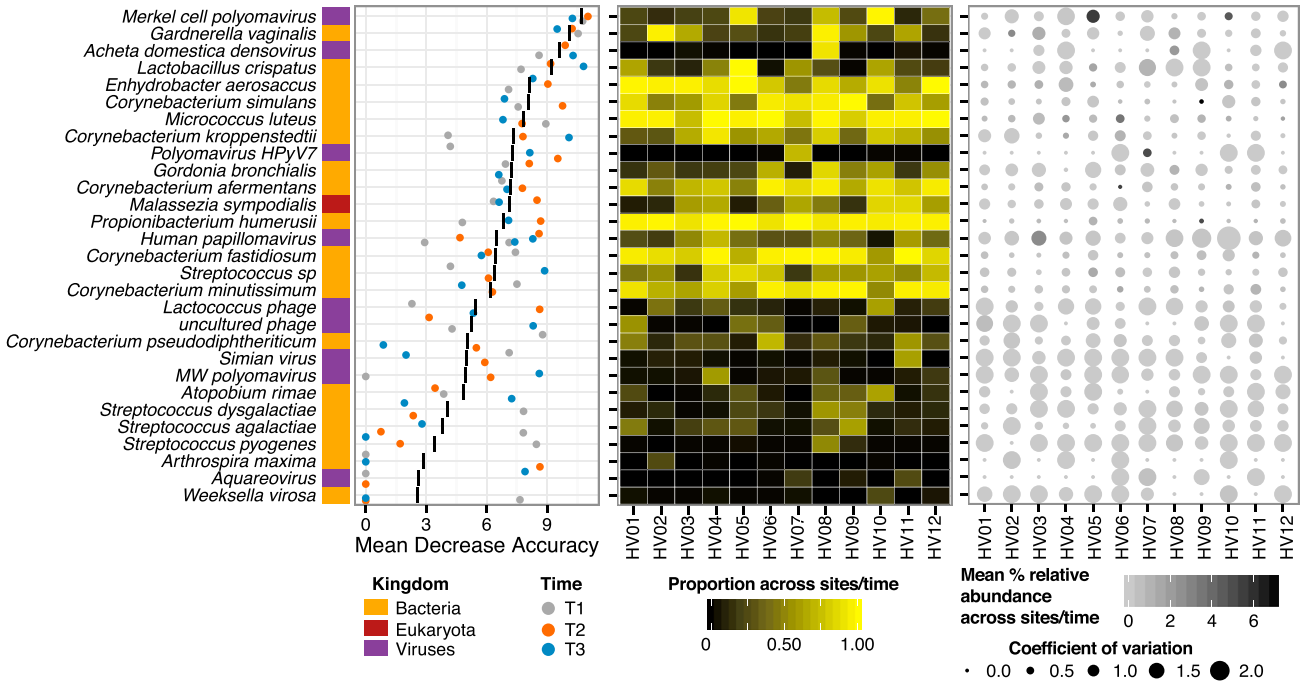

Figure 4. Individual-Specific Signature Taxa Are Shared across Time and Sites and Are Typically Low Abundance and Highly Stable

Left: variable importance plot of supervised random forest algorithm output. The top 30 taxa contributing to the model are shown on the y axis ranked by importance, quantified by the mean decrease in accuracy, that is, the degree to which inclusion of this predictor in model reduces classification error. The black line indicates the mean decrease in accuracy across the three time points; colored points indicate the score for each time point. Center: for each individual, the proportion of body sites for which each taxa is present is shown averaged across time points. Right: variation in mean relative abundance across sites and time points (color) with a coefficient of variation. HV, healthy volunteer.

See also Figure S3.

S. epidermidis. Strain heterogeneity could be unique to an individual (*P. acnes*) or specific to skin site (*S. epidermidis*) (Oh et al., 2014).

Here, we observed that *P. acnes* strains are remarkably stable over time across body sites (Figures 5A and S4A). We quantified this stability with the Yue-Clayton theta similarity index (Figure 5B), taking into account both strain presence/absence and relative abundance. Temporal stability, short- or long-term, surpassed the similarity between individuals, indicating that *P. acnes* stability likely derives from maintaining an individual's strains over time and less from the acquisition of new strains from the environment or other individuals.

To validate this hypothesis and to assess within-subject retention of strains, we also examined shared SNVs in the *P. acnes* genomes across the longitudinal samples. To power this analysis, we focused on two sebaceous sites, the manubrium and back, which have high-sequencing depth and *P. acnes* abundance (Figures S4C and S4D). For these sites, we used SNVs specific to the *P. acnes* core genome (2,248,676 bp region of the genome shared between all 78 sequenced strains) to ensure even representation of SNVs in every metagenomic sample. We identified 83,081 variant positions in the *P. acnes* core or ~24,000 SNVs per sample after filtering variants for an allele frequency >1% and >4 read depth. To test if the *P. acnes* sequencing depth was sufficient to identify the majority of variants, we generated rarefaction curves of SNVs discovered over increasing read depths (Figure 5C). We found that one million reads, 40× coverage of the *P. acnes* core, was sufficient for variant discovery.

The major advantage of an SNV-based approach is that given sufficient sequencing depth, temporal stability, and genetic diversity can be estimated in the absence of a large number of sequenced reference strains. By comparing the sharedness of SNVs between time points or individuals using the Jaccard index, which measures similarity based on presence/absence of features, we found the stability of *P. acnes* SNVs mirrors that of *P. acnes* strains over time (Figure 5B). We found that regardless of duration, an individual shares significantly more SNVs with themself over time than with other individuals (p value < 0.001).

Finally, polyallelism can reflect genetic heterogeneity, i.e., the presence of multiple strains, in a community. While the number of diallelic sites does not scale linearly with the number of strains in a sample, low levels are indicative of a monocolonized population. We focused on diallelic states, as triallelism was extremely rare (<1.0% in the population). We calculated the cumulative distribution of alternate alleles derived from the shotgun metagenomic reads as a function of distance from a defined reference genome (Figures 5D and S4E). Through these analyses, we identified a putatively monocolonized individual with strikingly low diallelism (1.0% of sites), in contrast to other individuals, e.g., HV02 and HV09, in which 97.4% and 25.6% of alternate sites

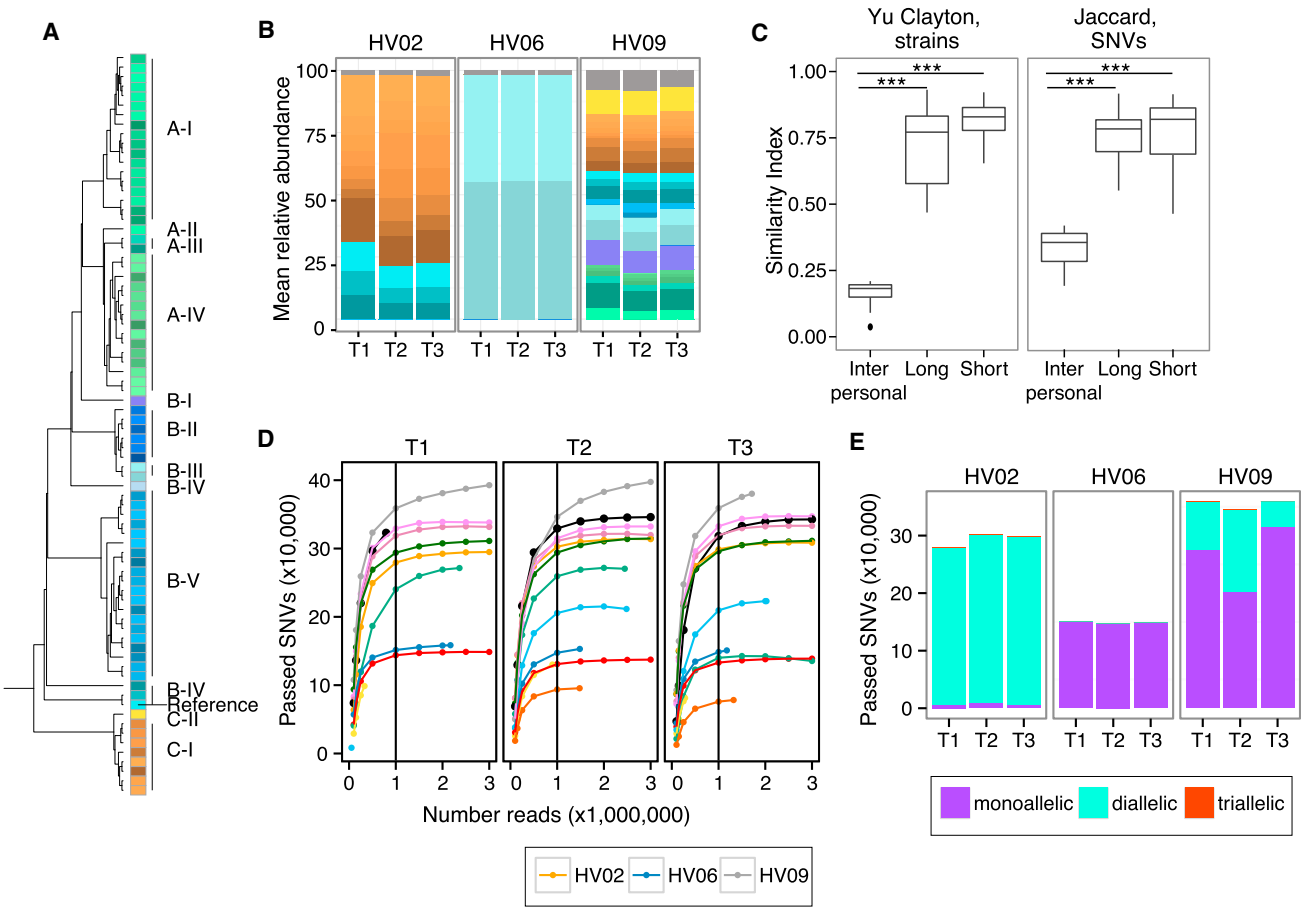

Figure 5. Individual-Specific Strain and SNV Signatures Are Stable over Time

(A) Dendrogram of *P. acnes* strain genome similarity based on core SNVs.

(B) *P. acnes* strain relative abundance plots of three representative individuals' manubrium; colors are as in (A). The full set of strain classifications is shown in Figure S6B.

(C) Boxplots of Yue-Clayton (left) and Jaccard (right) theta indices indicate similarity between strains (all body sites) and SNVs (manubrium and back) of *P. acnes* in a time series ($\theta = 1$ is identical). ***$p < 0.001$ value, Wilcoxon rank-sum test.

(D) Rarefaction curves demonstrate core SNV accumulation with read subsampling for manubrium sites. For remaining panels, SNVs are reported for samples subsampled to one million reads. Colors correspond to individuals as shown in Figure S1B.

(E) Number of SNVs that are mono-, di-, and triallelic. T1, T2, and T3 indicate order in the time series. HV, healthy volunteer.

See also Figure S4.

have reads reliably mapping to both reference and an alternate allele indicating the presence of multiple strains. For future disease studies, fluctuations in pollyallelism, for example, a dramatic decrease in the number of diallelic positions could indicate emergence of a dominant pathogenic strain.

P. acnes Pangenome Maximized across a Multi-phyletic Community

Since skin sites stably maintain the same *P. acnes* strains over time, we wanted to explore the community's full gene content to generate hypotheses about evolutionary forces shaping community drift, resilience, and stability on a functional level. The total functional repertoire of a species is the "pangenome," composed of core (conserved) and non-core (absent in at least one strain) genes. The *P. acnes* pangenome is composed of 3,774 non-redundant gene clusters, of which 1,685 were core (Figures S5A and S5B). Each additional genome adds three novel genes to the total (Figure S5C) (Tomida et al., 2013), implying that the majority of *P. acnes* functional capacity is captured within these 78 reference genomes. We mapped our reads to this *P. acnes* pangenome database, requiring one million reads for adequate sequencing depth (Figure S5D). Between 82.6% (3,117) and 99.9% (3,771) of the known *P. acnes* pangenome (Figure 6A) was represented in healthy individuals. 70% of samples had >95% (3,585) of the pangenome.

Interestingly, combining functional capacity with strain signatures revealed that similar pangenomic capacity can be achieved with distinct strain combinations (Figures 6A and 6B). This suggests that functional niche saturation can occur through multiple combinations of a limited number of strains, rather than requiring a full phylogenetic complement. Thus, while individuals have distinct *P. acnes* strain signatures, their functional

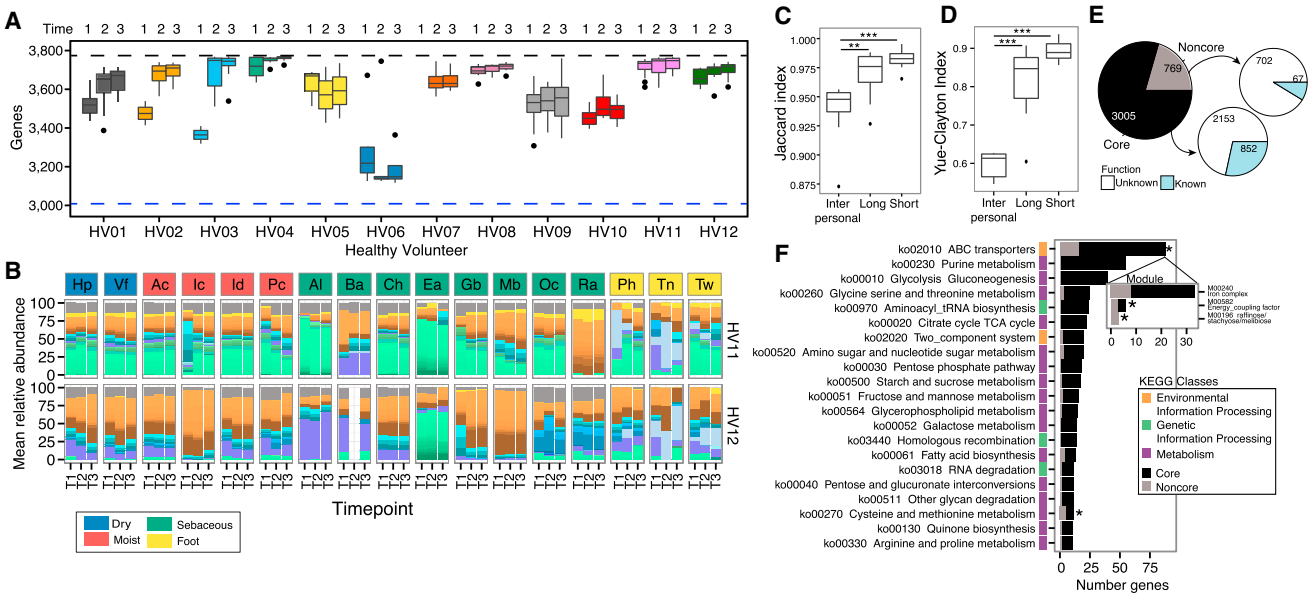

Figure 6. *P. acnes* Pangenome Reaches Functional Saturation with Distinct Strain Combinations

(A) Boxplots show the number of genes present at >40% coverage across sites of individuals at three time points. The black dashed line indicates the 3,774 genes in *P. acnes* pangenome. The blue dashed line indicates the 3,005 genes present in every individual at every time point in at least 50% of body sites. Sites with <1 million *P. acnes* reads were excluded.

(B) Relative abundance plots of *P. acnes* strains across all body sites, color-coded by site characteristic. Strain colors are defined in Figure 5A. T1, T2, and T3 indicate order in the time series.

(C) Boxplots of Jaccard theta indices indicate stability of gene presence over time ($\theta = 1$ is identical). $^{**}p < 0.01$, $^{***}p < 0.001$, Wilcoxon rank-sum test.

(D) Boxplots of Yue-Clayton theta indices indicate the stability of gene copy numbers over time ($\theta = 1$ means identical).

(E) Pie chart indicates the distribution of *P. acnes* genes between those present in all individuals "core" and those absent from some individuals "non-core." The majority of core and non-core genes are pathway "unknown" when compared to a KEGG database.

(F) Distribution of core and non-core genes for prevalent KEGG pathways. Colors indicate broader KEGG class of each pathway. Pathways with an asterisk are functionally enriched in non-core based on Fisher's exact test with a false discovery rate (FDR) < 0.05.

See also Figure S5.

capacities are remarkably similar, only differing 5% between individuals, and an individual is more likely to retain those unique genes over time (Figure 6C). This percent difference between individuals increases to ~40 when relative copy numbers of genes are compared (Figure 6D), further illustrating that while individuals' microbial communities have the same set of genes their relative abundances vary.

In addition to gene retention, we also observed an increase in pangenome size in three of the individuals (HV01, HV02, and HV03) over time (Figure 6A). Thus, although strain stability is more typical, individuals can acquire new gene content over time. Because of convergent functionality between individuals, we redefined the core genome to represent a "functional" core that is characteristic of healthy communities, toward which a probiotic approach might strive. We defined that 2,982 genes were present in at least 50% of sites in all individuals at all times, exceeding the 1,685 genes that are derived using genomes alone. This functional core genome increases to 3,186 genes when we exclude HV06 whose strain community is predominated by a single *P. acnes* clade (Figure S4A).

To evaluate functional enrichment within the 769 genes not identified as core, we assigned KEGG pathway annotations to clusters with BLAST. Unsurprisingly, these non-core genes were statistically enriched for pathway "none" (702 of 769 genes; Figure 6E), underscoring that more extensive gene annotations are needed to better understand functional variation. After removing unannotated clusters, we found accessory genes to be enriched in functions associated with ABC transporters and cysteine and methionine metabolism (Figure 6F). Ubiquitous across bacteria, ABC transporters facilitate communication between bacteria and the environment through the active transport of substances, such as ions, sugars, lipids, proteins, and drugs, across membranes, contributing to nutrient sensing and other processes.

Multi-phyletic *S. epidermidis* Communities Have More Variable Gene Content

To determine if our observations in *P. acnes* extended to other members of the skin community, we applied our analyses to evaluate the stability of S. *epidermidis* strains over time. Like *P. acnes*, *S. epidermidis* is a common skin commensal with well-documented sequence and gene content variation (Figure S6A). Multi-phyletic communities of *S. epidermidis* strains are stably maintained over time regardless of body site (Figures 7A and S6B); strain similarity over the long- and short-term exceeded similarity between individuals (p value < 0.001; Figure 7B), suggesting that new strains are rarely acquired from outside sources. Because *S. epidermidis* is maintained at an

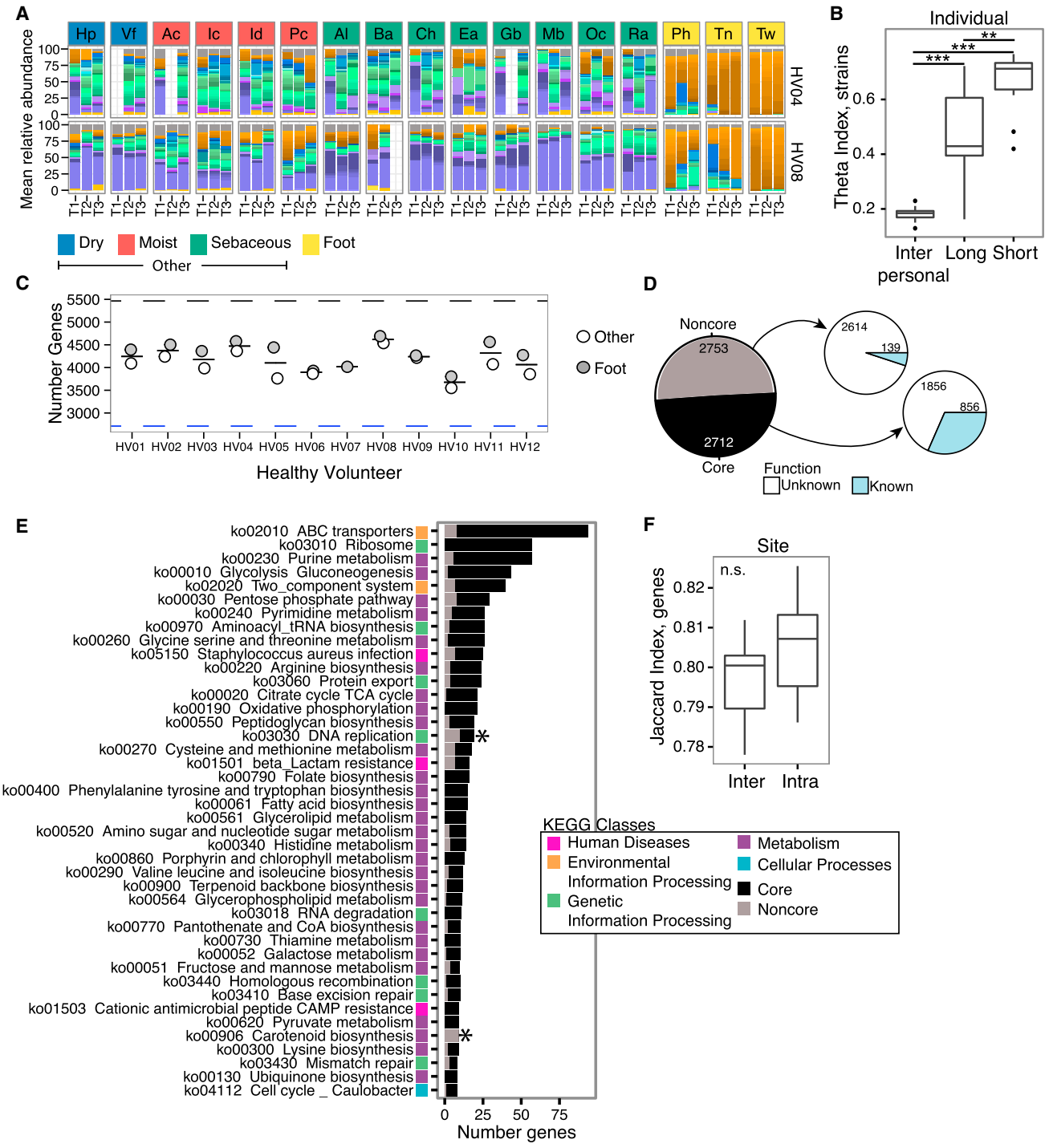

Figure 7. *S. epidermidis* Strains Remain Stable over Time, and Communities Do Not Reach Gene Saturation

(A) Relative abundance plots of *S. epidermidis* strains across body sites, color-coded by site characteristic. The full set of taxonomic classifications is shown in Figure S6B. Strain colors are defined in Figure S6A. Due to low coverage *S. epidermidis*, foot sites were combined as "foot," and all moist, dry, and sebaceous sites were combined as "other" (Figure S6E). Combined samples with <1 million *S. epidermidis* reads were excluded.

(B) Boxplots of theta indices indicate the stability of *S. epidermidis* strains within an individual over long or short time compared to between individuals (Inter) ($\theta = 1$ means identical). **$p < 0.01$; ***$p < 0.001$, Wilcoxon rank-sum test.

(C) The number of genes present on foot and other body sites, with the mean number shown as a thin bar. The black dashed line indicates the 5,465 genes present in *S. epidermidis* pangenome. The blue dashed lines indicate the 2,712 genes present in all foot and other combined samples.

(legend continued on next page)

overall lower abundance on the skin than *P. acnes* (<10% versus 40%), we lacked sufficient depth for SNV analyses.

The *S. epidermidis* pangenome, assembled from 61 reference genomes, is larger than that for *P. acnes*, containing 5,465 unique clusters and a non-core of 3,583 genes (Figure S6C) with 23 genes added from each additional genome (Figure S6D). To achieve sufficient coverage for pangenome analyses, S. *epidermidis* reads from three foot sites were pooled by individual to create "foot," while non-foot body sites were pooled to yield a composite "other" sample (Figure S6E). This grouping was based on B clade S. *epidermidis* dominance on all foot sites (Figure S6B). Using samples with greater than one million S. *epidermidis* reads (Figure S6F), we found that individuals did not appear to reach gene saturation and, generally, possessed from 65 to 85% (3,552 to 4,693 genes) of the available pangenome (Figure 7C). In addition to lower saturation of the pangenome, *S.epidermidis* gene content varied 20% between individuals, in contrast to 5% for *P. acnes*. Accordingly, our newly defined *S. epidermidis* healthy "core" is 2,712 genes. Unique genes could encode similar functions, but be unrecognized as homologs, which could increase the number of genes in the *S. epidermidis* pangenome, leading to lower full representation. However, the differences in the functional/gene saturation may also be explained by the relatively narrow niche of the sebaceous gland, where *P. acnes* primarily resides. *S. epidermidis* has a broader range, which could be reflected in the larger complement of genes needed for strains to persist in a niche.

To examine the functional diversity of the healthy non-core, we examined KEGG annotations for enrichment. Similar to *P. acnes*, the non-core was statistically enriched for pathway "none," with only 139 annotations for 2,753 genes (Figure 7D). Of annotated clusters, we identified DNA replication and carotenoid biosynthesis as enriched within the non-core (Figure 7E). Other enriched pathways demonstrated significant trends, including beta-lactam resistance, cysteine and methionine metabolism, bacterial secretion system, vancomycin resistance, and steroid hormone biosynthesis. Discovering multiple mechanisms of drug resistance in the non-core was unsurprising, given that individuals have varied histories of antibiotic usage and intraspecies transfer of drug resistance is common. Finally, we looked for functional differences in the foot compared to non-foot sites and found overall gene content was not statistically significantly different (Figure 7F), despite the presence of 212 genes specific to foot and 58 genes to non-foot sites.

DISCUSSION

Despite the continuous perturbation that human skin undergoes in daily life, healthy adults stably maintain their skin communities for up to 2 years, similar to the stability observed in the gut (Faith et al., 2013; Schloissnig et al., 2013). Homeostasis of skin microbial communities is largely maintained by fixation of abundant species, although a smaller number of low-abundance species are also stably maintained and contribute to an individual's unique microbial signature. We suspect that larger, longer-term studies will show a larger reservoir of transients entering and exiting the community, consistent with previous observations of individuals sharing and receiving microbes from the home and other individuals (Lax et al., 2014). Such stochastic drift likely increases over time, unless other constraints like geographic restriction, lifestyle, or host immune surveillance narrow the transient pool.

The exception to low-abundance transients was the class of DNA eukaryotic viruses, which displayed little sharedness across individuals and less site specificity than bacterial and fungal communities, which are strongly shaped by the nutritional availability, pH, and moisture of skin microenvironments. Eukaryotic viruses occupy a different niche (human cells) and interact with different constraints within the complex skin ecosystem. Interestingly, even high-abundance viral species were observed transiently, at least within the detection limits of metagenomic sequencing. This further supports a hypothesis for differential regulation and selection for eukaryotic viruses. However, viral communities are unusually complex to characterize due to technical limitations in recovery and classification; further computational and experimental approaches will be valuable to refine viral dynamics in the skin.

We surmise that in the absence of major perturbations, dominant characteristics of skin microbial communities would remain stable indefinitely, a conclusion previously extrapolated for gut communities (Faith et al., 2013; Schloissnig et al., 2013). This stability extends beyond the species level into SNVs and strains, which can impart unique functional contributions to a niche or individual. Total functional content variation, however, differed depending on skin species—*P. acnes*, a dominant skin commensal, showed low content variation in comparison to *S. epidermidis*. However, integration of metagenomic or "coding" potential with transcriptional or metabolomics profiles may better delineate community function, as SNVs and small variants can impact actual functional levels.

Future studies will define what and how extrinsic perturbations can alter the skin microbiota; these include antimicrobial treatment (e.g., Naik et al., 2012), probiotics, prebiotics, long-term environmental relocations, or diet (Kang et al., 2015). Intrinsic conditions like immunosuppression, illness, or the occurrence of disease have also been shown to cause major shifts in skin communities (Kong et al., 2012; Oh et al., 2013). In future disease studies, sequence data can generate hypotheses about which strains contribute to the disease and which are bystanders in the greater microbial consortia. Subsequently, valuable functional information can be gained from culturing and sequencing of primary isolates associated with metagenomic datasets.

(D) The pie chart indicates the distribution of *S. epidermidis* genes between those present in all individuals "core" and those missing from some individuals "non-core." The majority of core and non-core genes are pathway "unknown" when compared to a KEGG database.
(E) Distribution of genes between core and non-core for the most prevalent KEGG pathways. Colors indicate the broader KEGG class of each pathway. Pathways indicated with an asterisk are functionally enriched in non-core based on Fisher's exact test with a FDR < 0.05.
(F) *S. epidermidis* gene repertoire is not statistically more similar within a site (Intra) than between (Inter) sites, calculated with Jaccard theta.
See also Figure S6.

Functional assaying of individual and mixed strain groups in vitro and in animal models will be particularly relevant for determining the causality of diseases. Such studies are the prelude to prebiotic, probiotic, and transplantation approaches of skin microbes in the context of disease amelioration and prevention.

EXPERIMENTAL PROCEDURES

Subject Recruitment, Sampling, Processing, Sequencing, and Classification

Expanding our previous metagenomic survey, we resampled 12 healthy volunteers from our original study (Oh et al., 2014) approved by the institutional review board of the National Human Genome Research Institute (http://www.clinicaltrials.gov/ct2/show/NCT00605878). Longitudinal sampling occurred at 10–30 months ("long") and 5–10 weeks ("short") (Figure S1B). Recruitment criteria, sampling procedure, sample processing, sequencing, taxonomic classification, and strain tracking were as described previously, except for a new RefSeq viral genome database as of June 2015.

Identification of SNVs in the *P. acnes* Core

For high-coverage back and manubrium samples (Figure S4C), metagenomic reads were mapped against the *P. acnes* core genome, and the alignment file was processed with GATK's IndelRealigner (McKenna et al., 2010), samtools (Li, 2011), and bcftools to identify possible variants with criteria previously described (Lieberman et al., 2014).

Pangenome Analyses of Dominant Skin Species

As illustrated in Figure S5A, *P. acnes* and *S. epidermidis* nucleotide-coding sequences were clustered into non-redundant orthologs with usearch (Edgar, 2010) and validated with single-copy marker genes (Greenblum et al., 2015). A gene was considered present when 40% of its length was covered with reads (Zhu et al., 2015).

Statistics

All statistical analyses performed in R. Spearman correlations of non-zero values were used for all correlations. Supervised random forest models were implemented with the package randomForest (Liaw and Wiener, 2002). For all boxplots, center lines represent the median and the edges represent the first and third quartiles. The non-parametric Wilcoxon rank-sum test was used to determine statistically significant differences between populations. Statistical significance was ascribed to an alpha level of the adjusted p values ≤ 0.05. Similarity between samples was assessed using the Yue-Clayton theta or Jaccard similarity.

ACCESSION NUMBERS

The accession numbers and metagenomic read data reported in this paper have been uploaded to SRA under bioproject 46333.

SUPPLEMENTAL INFORMATION

Supplemental Information includes Supplemental Experimental Procedures, six figures, and five tables and can be found with this article online at http://dx.doi.org/10.1016/j.cell.2016.04.008.

AUTHOR CONTRIBUTIONS

J.O., A.L.B., H.H.K., and J.A.S. designed the study and drafted the manuscript. H.H.K. collected patient samples. Sequencing was carried out by NISC. J.O., A.L.B., and M.P. analyzed the sequence data.

ACKNOWLEDGMENTS

Amynah Pradhan, Sharon Osgood, Clay Deming, Cynthia Ng, Brian Schmidt, Pamela Thomas, and Sean Conlan provided underlying efforts; the J.A.S. lab and Mark Udey engaged in helpful discussions. Work was supported by NHGRI and NCI Intramural Research Programs and a Chanel/CE.R.I.E.S. research award (to J.A.S.). This study utilized the high-performance computational capabilities of the NIH Biowulf Linux cluster. Sequencing was funded by grants from the NIH (4UH3AR057504-02). IGS Analysis Engine at University of Maryland School of Medicine provided structural and functional annotation of genomes.

Received: November 10, 2015
Revised: January 21, 2016
Accepted: March 31, 2016
Published: May 5, 2016

REFERENCES

Alekseyenko, A.V., Perez-Perez, G.I., De Souza, A., Strober, B., Gao, Z., Bihan, M., Li, K., Methé, B.A., and Blaser, M.J. (2013). Community differentiation of the cutaneous microbiota in psoriasis. Microbiome *1*, 31.

Belkaid, Y., and Segre, J.A. (2014). Dialogue between skin microbiota and immunity. Science *346*, 954–959.

Caporaso, J.G., Lauber, C.L., Costello, E.K., Berg-Lyons, D., Gonzalez, A., Stombaugh, J., Knights, D., Gajer, P., Ravel, J., Fierer, N., et al. (2011). Moving pictures of the human microbiome. Genome Biol. *12*, R50.

Conlan, S., Mijares, L.A., Becker, J., Blakesley, R.W., Bouffard, G.G., Brooks, S., Coleman, H., Gupta, J., Gurson, N., Park, M., et al.; NISC Comparative Sequencing Program (2012). Staphylococcus epidermidis pan-genome sequence analysis reveals diversity of skin commensal and hospital infection-associated isolates. Genome Biol. *13*, R64.

Costello, E.K., Lauber, C.L., Hamady, M., Fierer, N., Gordon, J.I., and Knight, R. (2009). Bacterial community variation in human body habitats across space and time. Science *326*, 1694–1697.

Edgar, R.C. (2010). Search and clustering orders of magnitude faster than BLAST. Bioinformatics *26*, 2460–2461.

Faith, J.J., Guruge, J.L., Charbonneau, M., Subramanian, S., Seedorf, H., Goodman, A.L., Clemente, J.C., Knight, R., Heath, A.C., Leibel, R.L., et al. (2013). The long-term stability of the human gut microbiota. Science *341*, 1237439.

Findley, K., Oh, J., Yang, J., Conlan, S., Deming, C., Meyer, J.A., Schoenfeld, D., Nomicos, E., Park, M., Kong, H.H., and Segre, J.A.; NIH Intramural Sequencing Center Comparative Sequencing Program (2013). Topographic diversity of fungal and bacterial communities in human skin. Nature *498*, 367–370.

Flores, G.E., Caporaso, J.G., Henley, J.B., Rideout, J.R., Domogala, D., Chase, J., Leff, J.W., Vázquez-Baeza, Y., Gonzalez, A., Knight, R., et al. (2014). Temporal variability is a personalized feature of the human microbiome. Genome Biol. *15*, 531.

Franzosa, E.A., Huang, K., Meadow, J.F., Gevers, D., Lemon, K.P., Bohannan, J.M., and Huttenhower, C. (2015). Identifying personal microbiomes using metagenomic codes. Proc. Natl. Acad. Sci. USA *112*, E2930–E2938.

Gajer, P., Brotman, R.M., Bai, G., Sakamoto, J., Schütte, U.M., Zhong, X., Koenig, S.S., Fu, L., Ma, Z.S., Zhou, X., et al. (2012). Temporal dynamics of the human vaginal microbiota. Sci. Transl. Med. *4*, 132ra52.

Greenblum, S., Carr, R., and Borenstein, E. (2015). Extensive strain-level copy-number variation across human gut microbiome species. Cell *160*, 583–594.

Grice, E.A. (2015). The intersection of microbiome and host at the skin interface: genomic- and metagenomic-based insights. Genome Res. *25*, 1514–1520.

Grice, E.A., and Segre, J.A. (2011). The skin microbiome. Nat. Rev. Microbiol. *9*, 244–253.

Grice, E.A., Kong, H.H., Conlan, S., Deming, C.B., Davis, J., Young, A.C., Bouffard, G.G., Blakesley, R.W., Murray, P.R., Green, E.D., et al.; NISC Comparative Sequencing Program (2009). Topographical and temporal diversity of the human skin microbiome. Science *324*, 1190–1192.

Hannigan, G.D., Meisel, J.S., Tyldsley, A.S., Zheng, Q., Hodkinson, B.P., SanMiguel, A.J., Minot, S., Bushman, F.D., and Grice, E.A. (2015). The human skin double-stranded DNA virome: topographical and temporal diversity, genetic enrichment, and dynamic associations with the host microbiome. MBio *6*, e01578–15.

Human Microbiome Project Consortium (2012). Structure, function and diversity of the healthy human microbiome. Nature *486*, 207–214.

Kang, D., Shi, B., Erfe, M.C., Craft, N., and Li, H. (2015). Vitamin B12 modulates the transcriptome of the skin microbiota in acne pathogenesis. Sci. Transl. Med. *7*, 293ra103.

Kong, H.H., Oh, J., Deming, C., Conlan, S., Grice, E.A., Beatson, M.A., Nomicos, E., Polley, E.C., Komarow, H.D., Murray, P.R., et al.; NISC Comparative Sequence Program (2012). Temporal shifts in the skin microbiome associated with disease flares and treatment in children with atopic dermatitis. Genome Res. *22*, 850–859.

Lax, S., Smith, D.P., Hampton-Marcell, J., Owens, S.M., Handley, K.M., Scott, N.M., Gibbons, S.M., Larsen, P., Shogan, B.D., Weiss, S., et al. (2014). Longitudinal analysis of microbial interaction between humans and the indoor environment. Science *345*, 1048–1052.

Li, H. (2011). A statistical framework for SNP calling, mutation discovery, association mapping and population genetical parameter estimation from sequencing data. Bioinformatics *27*, 2987–2993.

Liaw, A., and Wiener, M. (2002). Classification and regression by randomForest. R News *2*, 18–22.

Lieberman, T.D., Flett, K.B., Yelin, I., Martin, T.R., McAdam, A.J., Priebe, G.P., and Kishony, R. (2014). Genetic variation of a bacterial pathogen within individuals with cystic fibrosis provides a record of selective pressures. Nat. Genet. *46*, 82–87.

Liu, J., Yan, R., Zhong, Q., Ngo, S., Bangayan, N.J., Nguyen, L., Lui, T., Liu, M., Erfe, M.C., Craft, N., et al. (2015). The diversity and host interactions of Propionibacterium acnes bacteriophages on human skin. ISME J. *9*, 2116.

Ma, Z.S. (2015). Power law analysis of the human microbiome. Mol. Ecol. *24*, 5428–5445.

McKenna, A., Hanna, M., Banks, E., Sivachenko, A., Cibulskis, K., Kernytsky, A., Garimella, K., Altshuler, D., Gabriel, S., Daly, M., and DePristo, M.A. (2010). The Genome Analysis Toolkit: a MapReduce framework for analyzing next-generation DNA sequencing data. Genome Res. *20*, 1297–1303.

Naik, S., Bouladoux, N., Wilhelm, C., Molloy, M.J., Salcedo, R., Kastenmuller, W., Deming, C., Quinones, M., Koo, L., Conlan, S., et al. (2012). Compartmentalized control of skin immunity by resident commensals. Science *337*, 1115–1119.

Oh, J., Freeman, A.F., Park, M., Sokolic, R., Candotti, F., Holland, S.M., Segre, J.A., and Kong, H.H.; NISC Comparative Sequencing Program (2013). The altered landscape of the human skin microbiome in patients with primary immunodeficiencies. Genome Res. *23*, 2103–2114.

Oh, J., Byrd, A.L., Deming, C., Conlan, S., Kong, H.H., and Segre, J.A.; NISC Comparative Sequencing Program (2014). Biogeography and individuality shape function in the human skin metagenome. Nature *514*, 59–64.

Peleg, A.Y., Hogan, D.A., and Mylonakis, E. (2010). Medically important bacterial-fungal interactions. Nat. Rev. Microbiol. *8*, 340–349.

Scharschmidt, T.C., and Fischbach, M.A. (2013). What lives on our skin: ecology, genomics and therapeutic opportunities of the skin microbiome. Drug Discov. Today Dis. Mech. *10*, 10.

Schloissnig, S., Arumugam, M., Sunagawa, S., Mitreva, M., Tap, J., Zhu, A., Waller, A., Mende, D.R., Kultima, J.R., Martin, J., et al. (2013). Genomic variation landscape of the human gut microbiome. Nature *493*, 45–50.

Tomida, S., Nguyen, L., Chiu, B.H., Liu, J., Sodergren, E., Weinstock, G.M., and Li, H. (2013). Pan-genome and comparative genome analyses of propionibacterium acnes reveal its genomic diversity in the healthy and diseased human skin microbiome. MBio *4*, e00003–e00013.

Yue, J.C., and Clayton, M.K. (2005). A similarity measure based on species proportions. Commun. Stat. A-Theor. *34*, 2123–2131.

Zhu, A., Sunagawa, S., Mende, D.R., and Bork, P. (2015). Inter-individual differences in the gene content of human gut bacterial species. Genome Biol. *16*, 82.

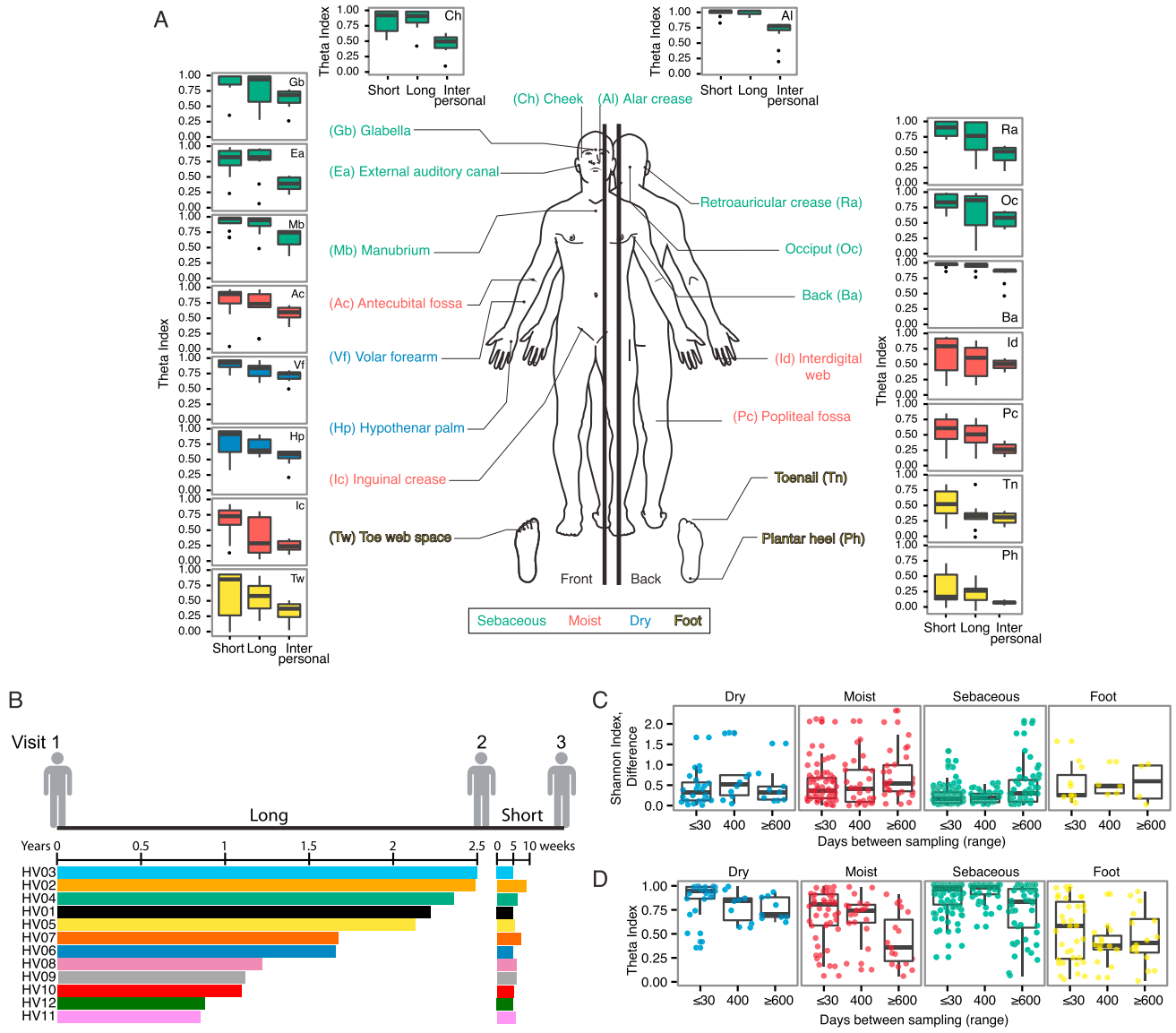

Figure S1. Study Characteristics and Design; Community Stability between Time Points, and the Effect of Days between Sampling, Related to Figure 1

(A) The 17 selected skin sites and their location on the human body. These sites represent four microenvironments: sebaceous (green), dry (blue), and moist (red), and foot (black). For all sites, boxplots of Yue–Clayton theta indices calculate similarity between samples in the time series, aggregated by the skin site characteristic. 'Long' duration indicates > 1 year between samplings; 'Short' duration averages a month. As comparison, 'Interpersonal' values show the average distance between individuals. Black lines indicate median, boxes show first and third quartiles. Panels are color coded by site characteristic. For all intra- versus inter-individual comparisons, $p < 0.05$ except for the Id ($p = 0.24$); for all long versus short comparisons, $p > 0.05$ except for the Ic ($p = 0.04$).

(B) Longitudinal study design to show time between samplings. Individuals' color bars are reference for individuals' lines in Figures 5D, S3A, S5D, S6F.

(C and D) Effect of time of sampling on (C) changes in diversity, and (D) community structure. 'Long' time points were divided into two groups, those that were ≥ 600 days ('600') between the first and second sampling, and those that were < 600 but ≥ 100 days between first and second sampling ('400'). Community structure was measured by the Yue-Clayton theta index and diversity with the Shannon diversity index. Black lines in boxplots indicate median, boxes show first and third quartiles. Site data are shown aggregated and colored by site characteristic. When analyzed by site, no comparison between '400' and '600' samples were statistically significant by a Wilcoxon-rank sum test, adjusted for multiple corrections.

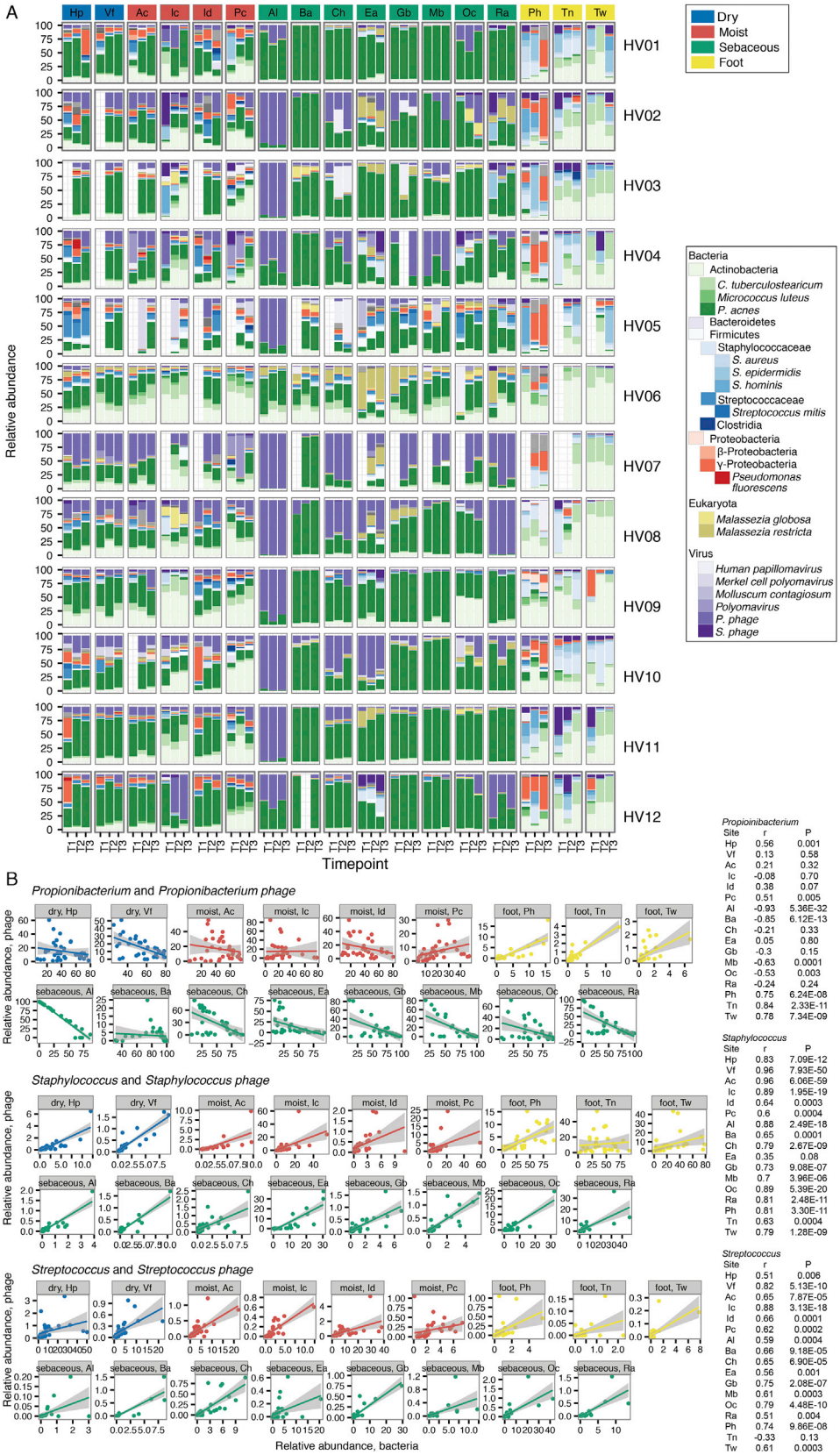

Propioinibacterium

Site	r	P
Hp	0.56	0.001
Vf	0.13	0.58
Ac	0.21	0.32
Ic	-0.08	0.70
Id	0.38	0.07
Pc	0.51	0.005
Al	-0.93	5.36E-32
Ba	-0.85	6.12E-13
Ch	-0.21	0.33
Ea	0.05	0.80
Gb	-0.3	0.15
Mb	-0.63	0.0001
Oc	-0.53	0.003
Ra	-0.24	0.24
Ph	0.75	6.24E-08
Tn	0.84	2.33E-11
Tw	0.78	7.34E-09

Staphylococcus

Site	r	P
Hp	0.83	7.09E-12
Vf	0.96	7.93E-50
Ac	0.96	6.06E-59
Ic	0.89	1.95E-19
Id	0.64	0.0003
Pc	0.6	0.0004
Al	0.88	2.49E-18
Ba	0.65	0.0001
Ch	0.79	2.67E-09
Ea	0.35	0.08
Gb	0.73	9.08E-07
Mb	0.7	3.96E-06
Oc	0.89	5.39E-20
Ra	0.81	2.48E-11
Ph	0.81	3.30E-11
Tn	0.63	0.0004
Tw	0.79	1.28E-09

Streptococcus

Site	r	P
Hp	0.51	0.006
Vf	0.82	5.13E-10
Ac	0.65	7.87E-05
Ic	0.88	3.13E-18
Id	0.66	0.0001
Pc	0.62	0.0002
Al	0.59	0.0004
Ba	0.66	9.18E-05
Ch	0.65	6.90E-05
Ea	0.56	0.001
Gb	0.75	2.08E-07
Mb	0.61	0.0003
Oc	0.79	4.48E-10
Ra	0.51	0.004
Ph	0.74	9.86E-08
Tn	-0.33	0.13
Tw	0.61	0.0003

(legend on next page)

Figure S2. Community Stability and Interactions at Species-Level Resolution, Related to Figure 2

(A) Full taxonomic classifications for all individuals, all sites. Sample headings are colored by site characteristic for each individual. Relative abundances of the most abundant skin taxa for each super-kingdom of bacteria, fungi, and viruses are shown. T1, T2, and T3 indicate time points, with T1 and T2 being long-duration time points (> 1 year) and T2 and T3 short-duration time points (~1 month).

(B) Phage and host dynamics for the three most abundant phages in skin. Correlation between relative abundances of a phage and its target bacterial genera for each sample. Plots are color coded by site characteristic. A linear model was fitted to the data with 95% confidence intervals for goodness of fit are shown in gray. Spearman correlation coefficients are shown in side tables.

Figure S3. Transience and Eukaryotic Viral Stability, Related to Figure 4

(A) Overall diversity trends of predicted eukaryotic virus species observed at > 1% genome coverage, over time. Different colors represent trends for different individuals. No site showed statistically significant changes in diversity over time (mixed effects model, adjusted $p > 0.05$).

(B) Non-phage classifications for major predicted DNA viruses for all individuals, all sites. Sample headings are colored by site characteristic for each individual. Most abundant viral classes are shown, with species predictions broken down by color.

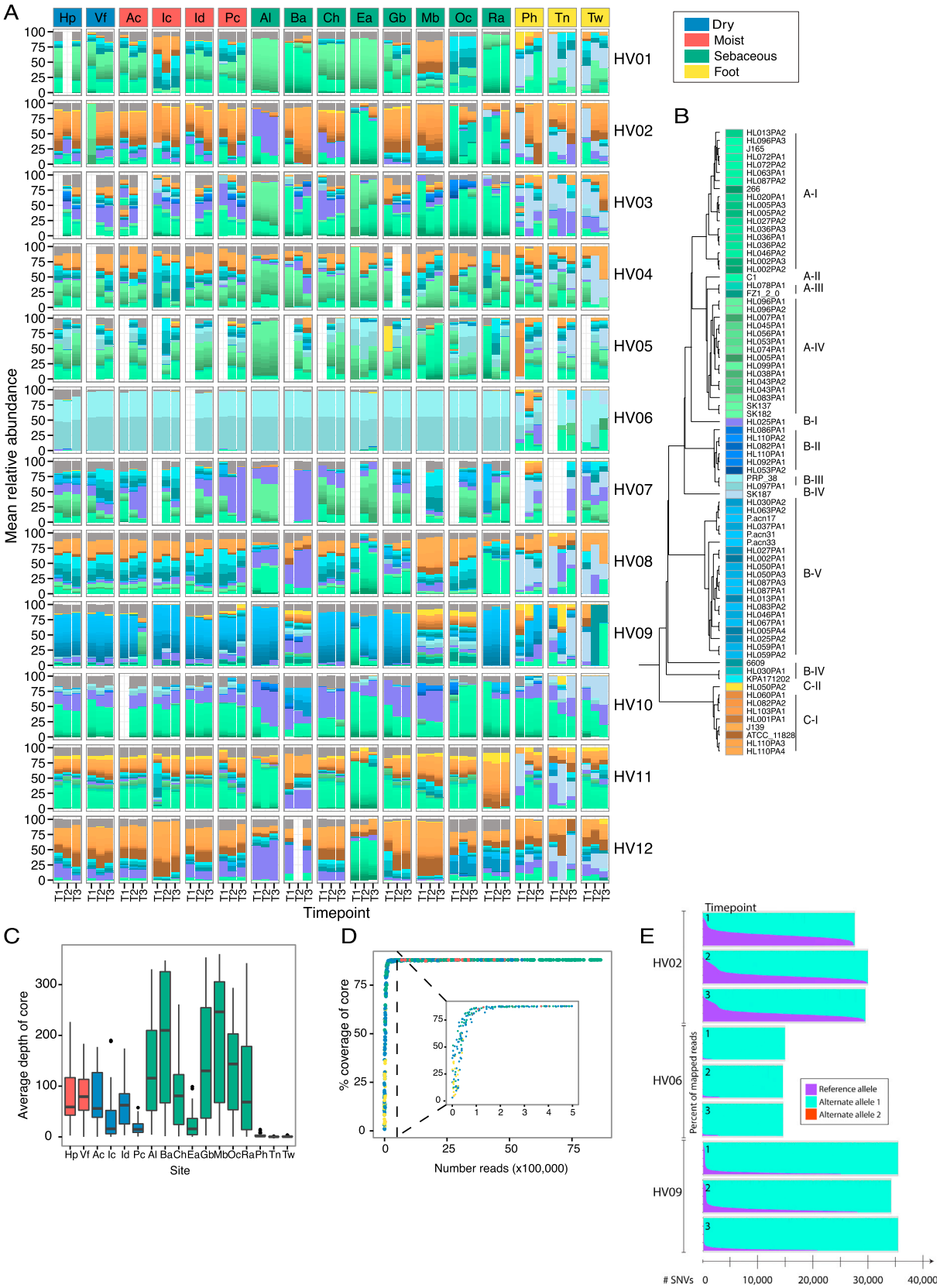

(legend on next page)

Figure S4. *P. acnes* Strains Are Stable over Time across Body Sites, Related to Figure 5

(A) Full *P. acnes* strain tracking for all individuals, all sites. Sample headings are colored by site characteristic. T1, T2, and T3 indicate time points, with T1 and T2 being long-duration time points (> 1 year) and T2 and T3 short-duration time points (~1 month). Colors correspond to those in (B).

(B) Dendrogram of *P. acnes* strain similarity based on core SNVs. Similar strains are grouped into clades.

(C) Boxplots show average depth of coverage of the *P. acnes* core across body sites. Black lines indicate median, boxes show first and third quartiles. Colors correspond to the site characteristic.

(D) Number of *P. acnes* reads versus percent coverage of the *P. acnes* core. With ~100,000 reads, the complete core is covered.

(E) For samples in (Figure 5A), the distribution of reads between the reference and alternate allele(s) for all identified SNVs. SNVs ordered by decreasing percentage of reads mapping to the reference allele.

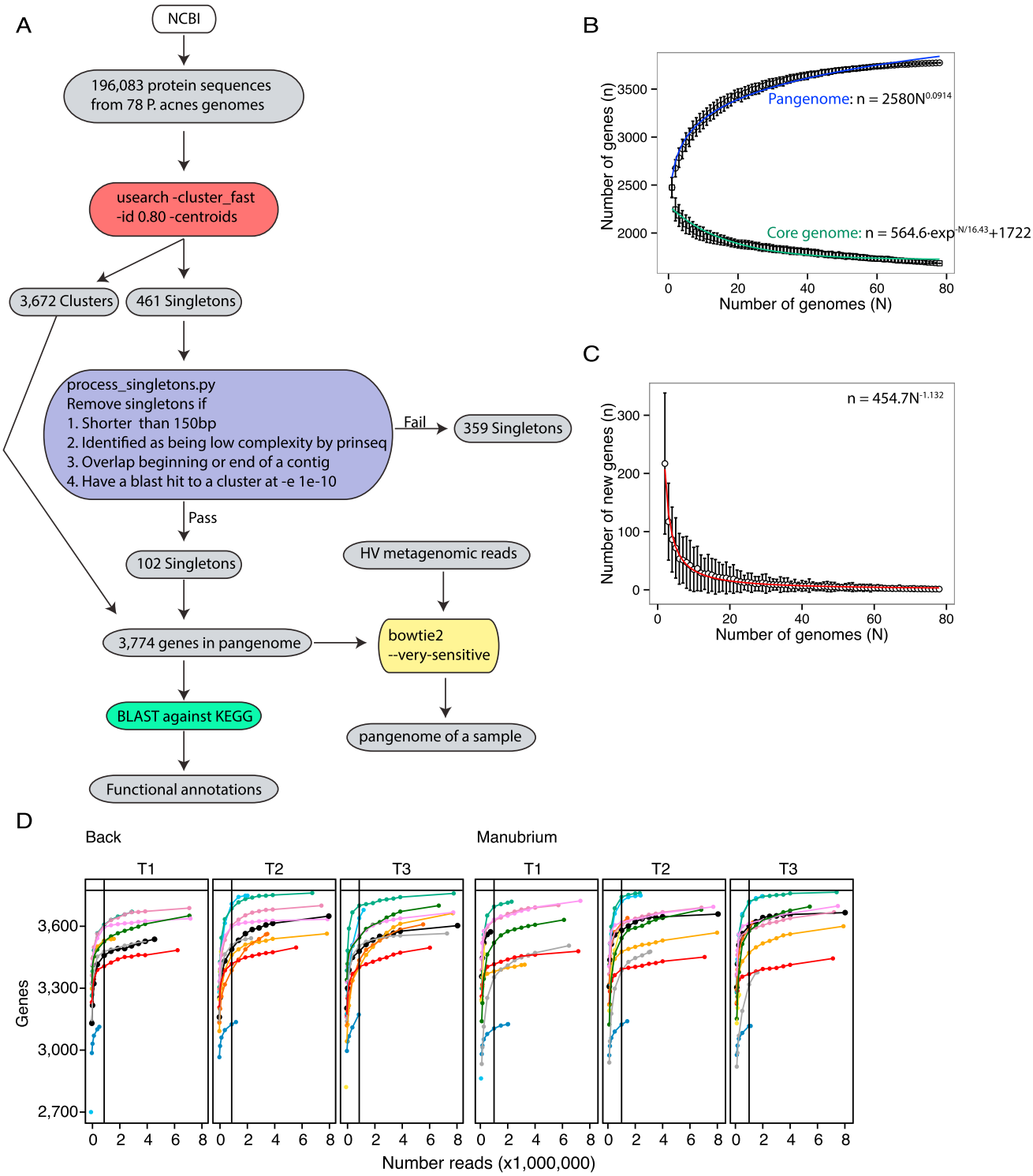

Figure S5. Pipeline for Pangenome Identification, Related to Figure 6

(A) Detailed pipeline for clustering of the *P. acnes* proteins. For all 78 *P. acnes* genomes, 196,083 protein annotations were downloaded from NCBI. All sequences were clustered with usearch into 3,672 clusters and 461 singletons. Singletons were filtered based on various criteria including length, complexity, and location. After filtering, 102 singletons remained for a total of 3,774 genes in the pangenome. These genes were then BLASTed against a KEGG database to assign functional annotation. Finally, the presence of the gene clusters in the metagenomic samples was determined using bowtie2.

(legend continued on next page)

(B) Gene accumulation curves for pangenome (blue) and core genome (green) as a function of genomes sequences (N). Pangenome data are fit by a power law regression. Core data are fit by an exponential decay curve. Points are means of n for 200 simulations. Error bars indicate the SDs for the 200 simulations.
(C) Accumulation of new genes (n) discovered with the addition of new genome sequences (N) fits a power law regression.
(D) Rarefaction curves for accumulation of genes for different size subsamples in representative sites. A minimum of 1 million reads was required for further pangenome analyses. Different colors represent trends for different individuals.

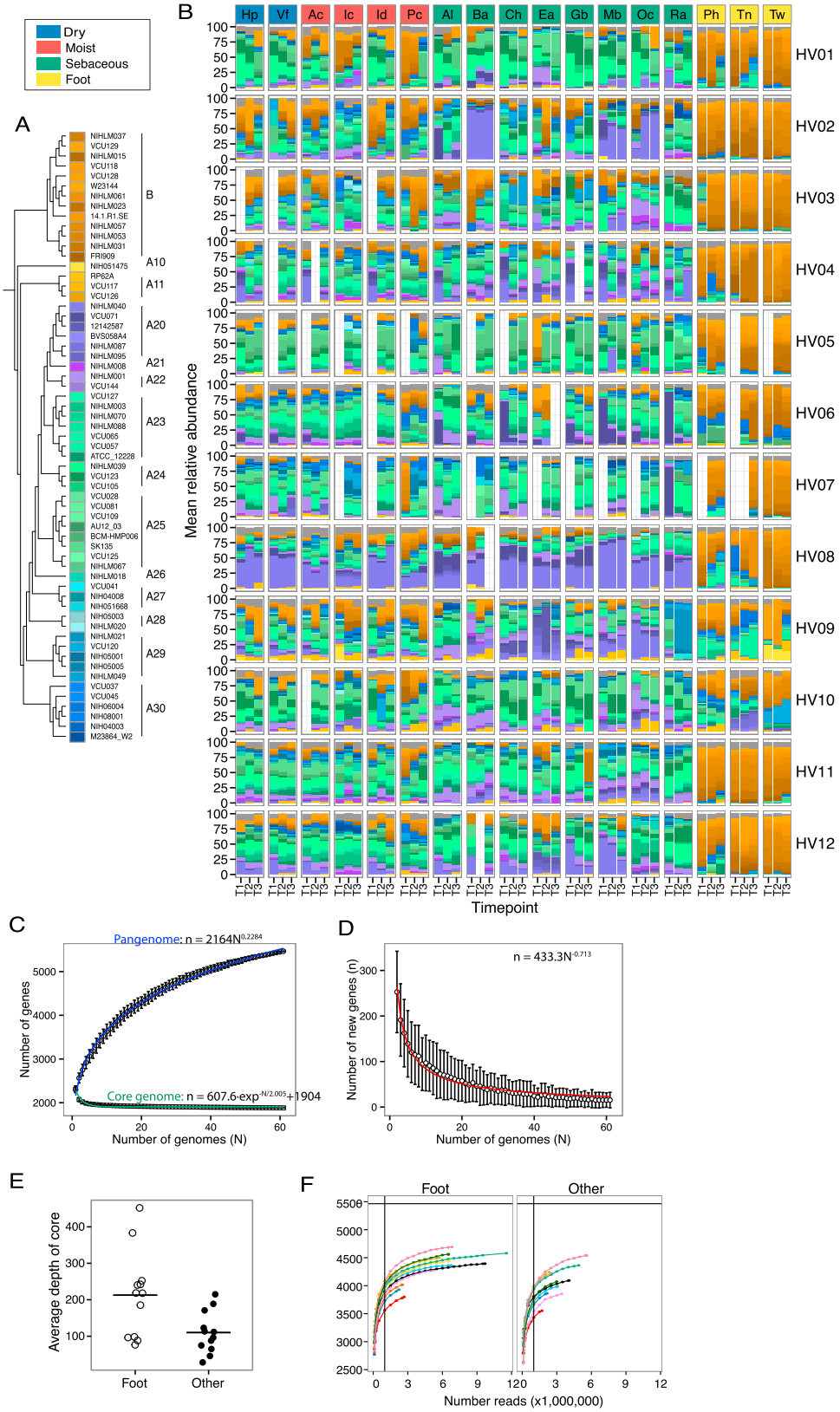

(legend on next page)

Figure S6. *S. epidermidis* Strains Are Stable over Time across Body Sites, Related to Figure 7

(A) Dendrogram of *S. epidermidis* strain similarity based on core SNVs. Similar strains are grouped into clades.

(B) Full *S. epidermidis* strain tracking for all individuals, all sites. Sample headings are colored by site characteristic. T1, T2, and T3 indicate time points, with T1 and T2 being long-duration time points (> 1 year) and T2 and T3 short-duration time points (~1 month). Colors correspond to those in (A).

(C) Gene accumulation curves for pangenome (blue) and core genome (green) as a function of genomes sequences (N). Pangenome data are fit by a power law regression. Core data are fit by an exponential decay curve. Points are means of n for 200 simulations. Error bars indicate the SDs for the 200 simulations.

(D) Accumulation of new genes (n) discovered with the addition of new genome sequences (N) fits a power law regression.

(E) Due to low *S. epidermidis* coverage across samples, all foot sites of an individual were combined as "foot" and all moist, dry, and sebaceous sites were combined as "other." Average depth of the *S. epidermidis* core for each sample is shown.

(F) Rarefaction curves for accumulation of genes for different size subsamples in the combined foot and other samples. A minimum of 1 million reads was required for further pangenome analyses. Different colors represent trends for different individuals.

Cell, Volume *165*

Supplemental Information

Temporal Stability of the Human Skin Microbiome

Julia Oh, Allyson L. Byrd, Morgan Park, Heidi H. Kong, Julia A. Segre, and NISC Comparative Sequencing Program

Supplemental Information

Experimental Procedures

Subject Recruitment and Sampling
To expand our previous metagenomic survey, we re-sampled 12 healthy volunteers from our original study (Oh et al., 2014). Recruitment criteria, sampling procedure, and sample processing were as described previously. Briefly, 7 males and 5 females adults <45 years without chronic skin diseases were sampled three times between June 2011 and May 2014. Sample collection was approved by the Institutional Review Board of the National Human Genome Research Institute (http://www.clinicaltrials.gov/ct2/show/NCT00605878) and all subjects provided informed consent. Longitudinal samples were collected such that the span between time 1 and time 2 was 10-30 months, while 5-10 weeks separated time 2 and time 3 (Figure S1B). This study design allowed the comparison of stability over a long and short time span. Individuals with a history of chronic medical conditions, including chronic dermatologic diseases, were excluded. 3 patients did report use of oral antibiotics between timepoint 1 and timepoint 2. However, in this study, antibiotic usage did not appear to induce discernible shifts in the overall diversity or structures of skin communities. Separate studies are necessary to fully understand the effects of oral antibiotics on the skin. Full sample characteristics are available in Table S1.

17 sites were sampled to represent the diverse physiological characteristics of skin and the sites of predilection for certain dermatologic disease (Figure S1A): dry (hypothenar palm, volar forearm), moist (antecubital crease, inguinal crease, interdigital web space, popliteal crease), sebaceous (alar crease, back, cheek, external auditory canal, glabella, manubrium, occiput, retroauricular crease), and foot (plantar heel, toenail, toe web space). To obtain sufficient DNA for metagenomic sequencing, most sites were sampled using a swab-scrape-swab procedure, exceptions include the external auditory canal where only a swab was used and the toenail where a clipping was taken. All samples were stored in lysis buffer at -80C until DNA extraction.

Sample Sequencing
Procedures for library generation, sequencing, and processing of longitudinal samples were as previously described (Oh et al., 2014). Briefly, Nextera library kits were used to generate Illumina libraries per manufacturer's instructions with the exception of increasing from 6 to 10 PCR cycles. Libraries were sequenced on an Illumina HiSeq at the NIH Intramural Sequencing Center to a target of 15 to 50 million clusters of 2 x 100bp reads. In total, for 12 individuals, 3 timepoints, we obtained 594 samples or 8.4 trillon reads (722 Gbp) of non-human, quality-filtered paired-end and singleton reads (median 17.9 million reads (1.4 Gbp) per sample). After human removal based on mapping to the hg19 human reference genome, all samples were processed to trim bases with quality score below 20 and remove reads less than 50 bp. To reduce computational burden, post quality control, samples with >20 million reads were subsampled to 10 million paired end reads, and singletons were discarded.

Taxonomic classification of skin species and diversity estimates.
Taxonomic classifications were performed as previously described (Oh et al., 2014), except we updated the viral database, incorporating all Refseq viral genomes as of 06.2015. The microbial reference genome database in total included 2342 bacterial, 389 fungal, 6009 viral, and 67 archaeal. Reads not matching hg19 + hg19 rRNA were mapped to this genome collection using bowtie2's —very-sensitive parameter retrieving the top 10 hits (Langmead and Salzberg, 2012). Reads mapping to multiple genomes were then reassigned using Pathoscope v1.0 (Francis et al., 2013), which uses a Bayesian framework to examine each read's sequence and mapping quality within the context of a global reassignment. Read hit counts were then normalized by genome length and scaled to sum to one. Coverages were calculated using the genomeCoverageBed tool in the Bedtools suite (Quinlan and Hall, 2010). Because very low abundance organisms are represented by few reads, they are more susceptible to misclassification than more abundant genomes. To reduce the effects of low abundance misclassifications, we used genome coverage cutoffs for relative abundance and diversity calculations; genomes were binned with coverage cutoffs of $\geq$ 1, 0.1, 0.01 or 0.001. A coverage cutoff of $\geq$ 1 was used for major analyses, a conservative number that produced classifications that most closely corresponded with the results from other common metagenomic classifiers (e.g., Metaphlan (Truong et al., 2015) or analysis using other methodologies like 16S rRNA and ITS gene sequencing (Oh et al., 2014). This number typically accounts for >99.9% of the community abundance. We used the Shannon

diversity index as well as species observed for diversity comparisons for bacterial classifications. All taxonomies were reconstructed to the species level, combining hits to multiple strain subtypes to reduce the potential for erroneous strain-calling (Table S2).

Strain tracking of dominant skin species

Strain tracking of the dominant skin commensals *Propionibacterium acnes* (Table S3) and *Staphylococcus epidermidis* (Table S5) was accomplished as described previously (Oh et al., 2014). Briefly, reference databases for *P. acnes* and *S. epidermidis* were compiled from all complete and draft genomes available on NCBI, 78 and 61, respectively. Whole genome alignment, with nucmer, was then used to identity the "core" region shared between all sequenced strains for a species. SNVs identified in these core regions were subsequently used to generate dendograms with PhyML 3.0. We then grouped strains into subtypes based on phylogenic distance, 12 for *P. acnes* and 14 for *S. epidermidis* (Figures S4B and S6B). Metagenomic reads were mapped to each species database with bowtie2 (-score-min L,-0.6,0.006, -k number of genomes) (Langmead and Salzberg, 2012) with zero tolerance for mismatches. The resulting alignment file was then processed with Pathoscope (-theta_prior 10 x 10^88) (Francis et al., 2013) to deconvolute multiple mapping reads. Accuracy of this strain-tracking approach was previously validated with extensive simulations (Oh et al., 2014).

Identification of SNVs in the P. acnes core

For each sample, coverage of the *P. acnes* core was calculated with samtools (Li, 2011) and genomecoveragebed (Quinlan and Hall, 2010). High average coverage nicely related to percent coverage of the *P. acnes* core (Figure S4). Back and manubrium samples had the highest *P. acnes* sequencing depth, so were selected for more extensive SNV analysis (Figure S4). Because *P. acnes* strains are shared across sites of an individual, these results can be extrapolated to the rest of the body. For SNV analysis, metagenomic reads were first mapped against the *P. acnes* core genome using bowtie2 (--very-sensitive). The resulting alignment file was sorted by samtools and then processed with GATK's IndelRealigner (McKenna et al., 2010) to minimize mismatches resulting from insertions or deletions in the reads with respect to the reference genome. The corrected alignment file was then analyzed with samtools and bcftools to identify possible variants (samtools mpileup -uD -q30 -Q30, bcftools view -Abvcg, vcfutils.pl varFilter -D99percentileofcoverage -d4 -1 .00001 -4 .00001). Parameters were selected to filter false positive polymorphisms that were a result of sequencing error, recent sequence duplications not found in the draft genome, strand bias, or end distance bias. Possible variants were then filtered with custom scripts to meet criteria previously described (Lieberman et al., 2014). Briefly, an alternate allele was only considered if it was supported by >2 reads with a minimum mapping quality of 30, had an allele frequency >3%, and fewer than 20% of reads supporting the SNV also mapped to an indel. With rarefaction curves of SNVs discovered over increasing read depths (Figure 5C), we found that 1 million reads, 40X coverage of the *P. acnes* core, was sufficient for variant discovery. Thus, to reduce computational burden only subsamples of 1 million reads were used for further analysis.

Pangenome analyses of dominant skin species

To identify the functional capacity of dominant species in our metagenomic samples, we followed the procedure illustrated in Figures S5A. First, 196,083 *P. acnes* nucleotide-coding sequences were downloaded from NCBI and 147,257 *S. epidermidis* sequences were extracted from Manatee annotations of the genomes. The IGS Analysis Engine was used for structural and functional annotation of the sequences. (http://ae.igs.umaryland.edu/cgi/index.cgi, Galens et al., 2011). Manatee was used to view annotations (http://manatee.sourceforge.net/). Genes were then clustered into non-redundant orthologs with usearch (-cluster_fast -id 0.80 -centroids) (Edgar, 2010). To validate accuracy of the clustering, we verified the presence of 13 single copy marker genes (Greenblum et al., 2015). Singletons, clusters composed of a single sequence, were then filtered based on previously established criteria (Lefebure and Stanhope, 2007). Briefly, singletons were excluded if they 1) were shorter than 150 nucleotides, 2) were flagged as low complexity by Prinseq (Schmieder and Edwards, 2011), or 3) overlapped the beginning or end of a contig. 4) had a blast hit to a cluster at -e 1e-10. Based on this criteria 359 *P. acnes* and 874 *S. epidermidis* singletons were removed, leaving 3,774 and 5,627 gene clusters respectively (Table S4 and Table S5, respectively). Gene accumulation curves for these clusters mirrored previous pangenome studies for *P. acnes* (Tomida et al., 2013) and *S. epidermidis (*Conlan et al., 2012*)*. The curves showed that new genes discovered with additional genomes and the pangenome followed a power law curve, while core genome size fit an exponential decay curve (Figure S5B,C, Figure S6C,D). These gene clusters were then annotated by BLASTx against the KEGG database. To identify the functional capacity of a sample, reads were mapped to each of the gene cluster databases using bowtie2 (--very-sensitive). A gene was subsequently considered present only when 40% of its length was covered with reads. This criteria reduces gene calling due to spuriously mapped reads or

reads from orthologs of closely related species (Zhu et al., 2015). Average coverage of each gene was calculated with samtools (Li, 2011) and then normalized by the average coverage of 13 single copy marker genes (Greenblum et al., 2015) to yield a copy number estimate.

Statistics

All statistical analyses were performed in the R software. Data are represented as mean ± standard error of the mean unless otherwise indicated. Spearman correlations of non-zero values were used for all correlation coefficients. Site characteristics were treated as separate groups where indicated based on spatial physiological differences between these different body niches (Grice et al., 2009). Supervised random forest models to identify discriminatory taxa and modules were implemented with the randomForest package in R (Liaw and Wiener, 2002). For all boxplots, black center lines represent the median and box edges the first and third quartiles. The nonparametric Wilcoxon rank-sum test was used to determine statistically significant differences between microbial populations. Unless otherwise indicated, P-values were adjusted for multiple comparisons using the p.adjust function in R using method = "fdr". Statistical significance was ascribed to an alpha level of the adjusted P-values ≤ 0.05. Similarity between samples was assessed using the Yue–Clayton theta or Jaccard similarity index with relative abundances of species, sub-strains, or shared genomic variants. The theta coefficient assesses the similarity between two samples based on (1) number of features in common between two samples, and (2) their relative abundances with $\theta = 0$ indicating totally dissimilar communities and $\theta = 1$ identical communities (Yue and Clayton 2005). As θ takes into account species abundance, it is less susceptible to low-abundance species whose classifications are less robust. The Jaccard similarity index is a metric defined by the union of the species occurring between two samples. To avoid repeated measures, samples belonging to an individual were averaged before statistical comparisons between site characteristic when using summary metrics such as means, diversity, or theta indices.

Supplemental References

Conlan, S., Mijares, L.A., NISC Comp Seq Program , Becker, J., Blakesley, R.W., Bouffard, G.G., Brooks, S., Coleman, H., Gupta, J., Gurson, N.*, et al.* (2012). Staphylococcus epidermidis pan-genome sequence analysis reveals diversity of skin commensal and hospital infection-associated isolates. Genome biology *13*, R64.

Edgar, R.C. (2010). Search and clustering orders of magnitude faster than BLAST. Bioinformatics *26*, 2460-2461.

Francis, O.E., Bendall, M., Manimaran, S., Hong, C., Clement, N.L., Castro-Nallar, E., Snell, Q., Schaalje, G.B., Clement, M.J., Crandall, K.A.*, et al.* (2013). Pathoscope: species identification and strain attribution with unassembled sequencing data. Genome research *23*, 1721-1729.

Galen, K., Orvis, J. Daugherty, S. Creasy, H.H., Angiuoli, S., White, O., Wortman, J., Mahurkar, A., Giglio, M.G., (2011). The IGS Standard Operating Procedure for Automated Prokaryotic Annotation. Stand Genomic Sci 4:244-251.

Greenblum, S., Carr, R., and Borenstein, E. (2015). Extensive strain-level copy-number variation across human gut microbiome species. Cell *160*, 583-594.

Grice, E.A., Kong, H.H., Conlan, S., Deming, C.B., Davis, J., Young, A.C., NISC Comp Seq Program, Bouffard, G.G., Blakesley, R.W., Murray, P.R.*, et al.* (2009). Topographical and temporal diversity of the human skin microbiome. Science *324*, 1190-1192.

Langmead, B., and Salzberg, S.L. (2012). Fast gapped-read alignment with Bowtie 2. Nature methods *9*, 357-359.

Li, H. (2011). A statistical framework for SNP calling, mutation discovery, association mapping and population genetical parameter estimation from sequencing data. Bioinformatics *27*, 2987-2993.

Liaw, A., and Wiener, M. (2002). Classification and regression by randomForest. R News *2*, 18-22.

Lieberman, T.D., Flett, K.B., Yelin, I., Martin, T.R., McAdam, A.J., Priebe, G.P., and Kishony, R. (2014). Genetic variation of a bacterial pathogen within individuals with cystic fibrosis provides a record of selective pressures. Nature genetics *46*, 82-87.

McKenna, A., Hanna, M., Banks, E., Sivachenko, A., Cibulskis, K., Kernytsky, A., Garimella, K., Altshuler, D., Gabriel, S., Daly, M.*, et al.* (2010). The Genome Analysis Toolkit: a MapReduce framework for analyzing next-generation DNA sequencing data. Genome research *20*, 1297-1303.

Oh, J., Byrd, A.L., Deming, C., Conlan, S., Program, NISC Comp Seq Program, Kong, H.H., and Segre, J.A. (2014). Biogeography and individuality shape function in the human skin metagenome. Nature *514*, 59-64.

Quinlan, A.R., and Hall, I.M. (2010). BEDTools: a flexible suite of utilities for comparing genomic features. Bioinformatics *26*, 841-842.

Schmieder, R., and Edwards, R. (2011). Quality control and preprocessing of metagenomic datasets. Bioinformatics *27*, 863-864.

Tomida, S., Nguyen, L., Chiu, B.H., Liu, J., Sodergren, E., Weinstock, G.M., and Li, H. (2013). Pan-genome and comparative genome analyses of propionibacterium acnes reveal its genomic diversity in the healthy and diseased human skin microbiome. mBio *4*, e00003-00013.

Truong, D.T., Franzosa, E.A., Tickle, T.L., Sholz, M., Weingart, G., Passolli, E., Tett, A., Huttenhower, C., Segata, N. (2015). MetaPhlAn2 for enhanced metagenomic taxonomic profiling.Nature methods 12:902-903.

Yue, J. C., Clayton, M. K. (2005) A similarity measure based on species proportions. Comm. Statist. Theory Methods 34, 2123–2131.

Zhu, A., Sunagawa, S., Mende, D.R., and Bork, P. (2015). Inter-individual differences in the gene content of human gut bacterial species. Genome biology *16*, 82.